DEVELOP MULTI-SCALE ENERGY AND EMISSION MODELS

Final Report

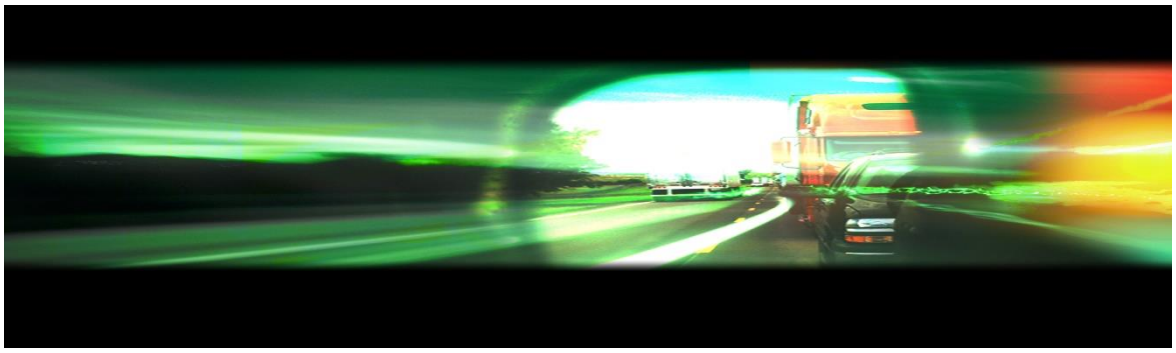

TranLIVE

Hesham Rakha, Jinghui Wang and Mohamed Abdelmegeed

November 2016

DISCLAIMER

The contents of this report reflect the views of the authors, who are responsible for the facts and the accuracy of the information presented herein. This document is disseminated under the sponsorship of the Department of Transportation, University Transportation Centers Program, in the interest of information exchange. The U.S. Government assumes no liability for the contents or use thereof.

1. Report No.	2. Government Accession No.	3. Recipient's Catalog No.
4. Title and Subtitle Develop Multi-scale Energy and Emission Models		5. Report Date November 2016
		6. Performing Organization Code KLK900-SB-002
7. Author(s) Rakha, Hesham; Wang, Jinghui; Abdelmegeed, Mohamed		8. Performing Organization Report No. N17-01
9. Performing Organization Name and Address National Institute for Advanced Transportation Technology University of Idaho PO Box 440901; 115 Engineering Physics Building Moscow, ID 83844-0901		10. Work Unit No. (TRAIS) 11. Contract or Grant No. DTRT12GUTC17
12. Sponsoring Agency Name and Address US Department of Transportation Research and Special Programs Administration 400 7th Street SW Washington, DC 20509-0001		13. Type of Report and Period Covered Final Report: 1/1/2012 – 11/30/2016 14. Sponsoring Agency Code USDOT/RSPA/DIR-1
15. Supplementary Notes:		

16. Abstract

The study develops energy consumption and emission models for multiple vehicle modes and rail transit trains in support of environmentally sustainable transportation systems (e.g. eco-routing, eco-driving, eco-transit, eco-freight). Specifically, electric light duty vehicles (LDVs) and trains, conventional diesel, hybrid-electric and compressed natural gas (CNG) buses as well as heavy duty diesel trucks are thoroughly investigated. The models are developed based on Virginia Tech Comprehensive Power-based Fuel consumption Model (VT-CPFM) for fuel-powered vehicles and Virginia Tech Comprehensive Power-based electric vehicle Energy consumption Model (VT-CPEM) for electric energy vehicles and trains. The models can circumvent the bang-bang control in the modeling practice and also can be easily calibrated using publicly available data. The validation efforts are made by instantaneously comparing estimated energy/fuel consumption against field observations and/or the estimates of other state-of-the-art models. The results demonstrate that the proposed models can accurately predict energy/fuel consumption and emissions consistent with field measurements.

17. Key Words Eco-routing, Eco-driving, energy consumption, emission, multi-modal	18. Distribution Statement Unrestricted; Document is available to the public through the National Technical Information Service; Springfield, VT.

19. Security Classif. (of this report) Unclassified	20. Security Classif. (of this page) Unclassified	21. No. of Pages #33	22. Price …

Form DOT F 1700.7 (8-72) Reproduction of completed page authorized

TABLE OF CONTENTS

EXECUTIVE SUMMARY

The study develops energy consumption and emission models for multiple vehicle modes and rail transit trains in support of environmentally sustainable transportation systems, such as eco-routing, eco-driving, eco-transit, and eco-freight systems. Given that conventional gasoline-powered light duty vehicles (LDVs) have been modeled by previous studies [1, 2], the proposed study mainly focuses on Heavy Duty Vehicles (HDVs), alternative fuel vehicles and rail trains. Specifically, electric LDVs and trains, conventional diesel, hybrid-electric and compressed natural gas (CNG) buses as well as heavy duty diesel trucks are thoroughly investigated.

The models are developed based on Virginia Tech Comprehensive Power-based Fuel consumption Model (VT-CPFM) for fuel-powered vehicles and Virginia Tech Comprehensive Power-based electric vehicle Energy consumption Model (VT-CPEM) for electric energy vehicles and trains. The VT-CPFM modeling framework characterizes fuel consumption as a second-order polynomial function of vehicle power so that circumvent the bang-bang control in the modeling practice. A bang-bang control suggests that a driver has to accelerate the vehicle at ‘‘full throttle” or decelerate at ‘‘full braking” to achieve the minimum fuel consumption level, which is not realistic. The VT-CPEM modeling framework models the electric energy consumption as a polynomial function of vehicle speed and acceleration, and also instantaneously captures the energy regeneration resulting from braking by characterizing the regenerative efficiency as an exponential function of deceleration level. The models are validated by comparing estimated fuel/energy consumption and emissions against field observations and/or the estimates of other state-of-the-art models. The results demonstrate that the proposed models can accurately predict energy/fuel consumption and emissions consistent with field measurements. The resulting models will be used to develop eco-friendly strategies for multimodal transportation systems.

This research effort resulted in the following peer-reviewed publications:

1. Wang, J. and Rakha, H.A., 2016. Fuel consumption model for conventional diesel buses. *Applied Energy*, 170, pp.394-402.
2. Fiori, C., Ahn, K. and Rakha, H.A., 2016. Power-based electric vehicle energy consumption model: Model development and validation. *Applied Energy*, 168, pp.257-268.
3. Wang, J. and Rakha, H.A., 2016. Modeling Fuel Consumption of Hybrid Electric Buses: Model Development and Comparison with Conventional Buses. *Transportation Research Record: Journal of the Transportation Research Board*, (2539), pp.94-102.
4. Wang, J. and Rakha, H.A., 2016. Heavy-Duty Diesel Truck Fuel Consumption Modeling. In *Transportation Research Board 95th Annual Meeting* (No. 16-2147).
5. Abdelmegeed, M., Rakha, H.and Ahn., K. 2016. Modeling Light Duty Vehicle Emissions Exploiting VT-CPFM Fuel Estimates. Presented at *Transportation Research Board 95th Annual Meeting*.
6. Abdelmegeed, M. and Rakha, H. K. 2016. Heavy-Duty Diesel Truck Emission ModelingModeling Light Duty Vehicle Emissions Exploiting VT-CPFM Fuel Estimates. Presented at *Transportation Research Board 96th Annual Meeting*.

PROBLEM OVERVIEW

Transportation has become one of the major contributors to energy consumption and emissions production. As demonstrated by [3, 4], transportation activities account for 28% of the total U.S. energy use and 33.4% of carbon dioxide (CO_2, the major component of GHG emissions) production. Furthermore, the energy use also results in severe air pollution (e.g. HC, CO, NO_x), significantly deteriorating air quality and dwelling environment. The intensification of global energy security, climate change and air pollution stimulates the development of innovative strategies to reduce energy consumption and emissions from the transportation sector. Towards this motivation, accurate, efficient and simple models are needed to provide robust estimates in support of quantifying potential reductions in energy/fuel consumption and emission levels induced by implementing eco-friendly strategies.

Among the existing modeling efforts for conventional fuel-powered vehicles, most are operated at a macroscopic or microscopic level. The macroscopic models, such as MOBILE 6.2 [5], were demonstrated to produce unreliable estimates due to their inability of capturing transient vehicle activities [6]. Consequently, they are incapable of being utilized for the energy and environmental assessment of traffic operational projects. Microscopic models were introduced in order to better capture the variability associated with vehicle dynamics. A wide range of instantaneous models have been developed using in-laboratory or field data, such as MOVES, VT-Micro [7], the Passenger Car and Heavy Duty Emission Model (PHEM) [8], VERSIT [9], the Comprehensive Modal Emissions Model (CMEM) [10, 11]. The majority of the aforementioned models, however, have limitations in use. For example, MOVES, which was developed as an inventory model based on a wide range of data sources, is capable of providing robust estimates. Nonetheless, it requires massive user inputs for each run, which significantly increases the time required to run multiple scenarios and large networks. CMEM generally underestimates fuel consumption levels for acceleration maneuvers; more importantly, it characterizes fuel consumption as a linear function of vehicle power, which produces a bang-bang type of control system. A bang-bang control may arise when the partial derivative of the response with respect to the control variable is not a function of the control variable, resulting in that drivers have to accelerate the vehicle at ‘‘full throttle” or decelerate at ‘‘full braking” to achieve the minimum fuel consumption level, which is not correct in reality. PHEM and VERSIT also produce a bang-bang control. VT-Micro is capable of circumventing the bang-bang control; however, it requires a large amount of in-laboratory or field data to be calibrated, which is cost-prohibitive and time-consuming. The existing fuel consumption models either produce a bang–bang type of control system or cannot be easily calibrated or efficiently used. Consequently, a simple, accurate and efficient model is needed.

For electric-powered vehicles, they are expected to gain a significant market share in the near future to reduce fossil fuel use and GHG emissions and to mitigate air pollution. Extensive studies performed by the University of California, Berkeley predict that approximately 2.5 million Electric Vehicles (EVs) will be present on American roads by 2020 [12]. The introduction of EVs will significantly reduce vehicle fuel consumption and emission levels. In order to quantify the network-wide impacts of EVs, there is a need to develop simple and accurate electric energy consumption models. This study partly attempts to address this need by developing the modeling framework applicable to both on-road

vehicles and rail trains that can be easily calibrated and implemented in transportation simulation software and in-vehicle and Smartphone eco-driving and eco-routing applications.

A number of models have been developed to estimate EVs or Electric Trains (ETs) energy consumption levels. For EVs, Muratori et al. [13] proposed a model centered on the estimation of the total primary energy consumption associated with personal transportation in the U.S. including different vehicle types to evaluate the impact of plug-in electric vehicles on the electric power grid at the distribution level. In particular, three main modeling steps were introduced: modeling of the behavior of drivers, generating realistic driving profiles, and simulating energy consumption of different vehicle types. Wu et al. [14] in their study first present a system which can collect in-use EV data and vehicle driving data. Approximately 5 months of EV data were collected and these data were used to analyze both EV performance and driver behavior. The analysis showed that EVs are more efficient when driving on in-city routes than driving on freeway routes. Based on the analysis results, an analytical EV power estimation model is developed. Hayes et al. [15] developed simplified EV models to quantify the impact of battery degradation with time and vehicle HVAC loads on the total vehicle energy consumption. The models were compared with published manufacturer specifications under various route and driving conditions, and for various driving cycles. Shibata et al. [16] and Abousleiman et al. [17] in their papers evaluate the energy consumption of an EV considering a constant regenerative braking efficiency. Halmeaho et al. [18] developed an analysis focused on an Electric City Bus Energy Flow Model but in this study the magnitude of the regenerative braking is limited due to the effective powertrain capacity, traction and eventually the bus stability. For ETs, most widely available measures are those estimated on an annual gross average basis [19, 20], which are not capable of representing the discrepancy of energy efficiency associated with route and vehicle characteristics, passenger loading, speed profiles and weather and track conditions. Some of the researchers [21-25] developed the models sensitive to the aforementioned system characteristics; however, they failed to capture instantaneous energy regeneration.

Though there have been numerous studies on the modeling of EVs or ETs energy consumption, these studies were of limited application. For example, they either focused on macro-project evaluations or simplified well-to-wheels analyses. None of these models were developed in a manner that would allow them to be applied without collecting vehicle-specific data while at the same time accurately model vehicle transient behavior, model energy regeneration at a microscopic level, and are simple enough to be incorporated within traffic simulation software or Smartphone applications. The proposed EV and ET energy models were developed to address this urgent need.

In a nutshell, the study is motivated to develop accurate, simple and efficient fuel/energy consumption and emission models which circumvent the bang-bang control and can be easily calibrated using readily available data and also can be efficiently implemented in traffic simulation software or Smartphone applications.

APPROACH AND METHODOLOGY

Conventional diesel, hybrid-electric and compressed natural gas (CNG) buses as well as heavy duty diesel trucks were modeled using VT-CPFM modeling framework, and electric LDVs and trains were modeled using the VT-CPEM framework [26].

VT-CPFM modeling framework

As a power-based model, the VT-CPFM framework uses a bottom-up approach. Namely, the parameters, such as resistance force, used for power estimation are first computed by a resistance force module; and thereafter the vehicle power is estimated with an engine power module which characterizes the vehicle power as a function of the resistance forces. The fuel consumption is then estimated using a fuel rate module that models the fuel consumption as a polynomial function of the vehicle power. Finally, the emissions for HC, CO, NO_x were mathematically characterized as a function of fuel consumption and speed.

The resistance force is computed considering a combination of aerodynamic, rolling, and grade resistance forces, as expressed in Eq.(1):

$$\mathbf{R(t)} = \frac{\rho}{25.92} C_d C_h A_f v(t)^2 + 9.8066 m \frac{C_r}{1000}(c_1 v(t) + c_2) + 9.8066 m G(t) \quad (1)$$

where R(t) is the vehicle resistance force (N); ρ is the air density at sea level at a temperature of 15 ℃ (59 ℉) (equal to 1.2256 kg/m^3); C_d is the drag coefficient (unitless) which is determined by truck type, 0.78 is used for the tested trucks (no aerodynamic aids) in this study [27]; C_h is the correction factor for altitude (unitless), calculated by 1-0.085H (H is the altitude in km); A_f is the frontal area of trucks (m^2), 10.7 m^2 is used based on the truck type; v(t) is the velocity in km/h; m is the vehicle mass in kg; Cr, c_1 and c_2 are the rolling resistance parameters (unitless), which vary as a function of road surface type and conditions as well as vehicle tire type; their typical values could be obtained from [27, 28]. G(t) is the instantaneous road grade which is determined by elevation profiles.

The power exerted at any instant t is formulated by [29] as expressed in Eq.(2):

$$\mathbf{P(t)} = \frac{R(t) + (1 + \lambda + 0.0025 \xi v(t)^2) m a(t)}{3600 \eta} v(t) \quad (2)$$

where P(t) is the vehicle power in *kW*; λ is the mass factor accounting for rotational masses, a value of 0.1 is used for heavy duty vehicles (HDVs) [30, 31]; ξ is the gear ratio and assumed to be zero in this paper due to the lack of engine gear data. a(t) is the instantaneous acceleration (m/s^2); η is the driveline efficiency.

The general structure of the fuel consumption model was specified as a two-regime mechanism. Rakha et al. [2] developed two VT-CPFM frameworks (VT-CPFM-1 and VT-CPFM-2) each of which is a two-regime model and characterizes fuel consumption as a second-order polynomial function of vehicle power. The use of a second order model ensures that a bang-bang control does not result from the application of the model. Furthermore, the model higher than second-order may not be calibrated using standard drive cycles given the complexity of the higher order model. Consequently, a second-order model achieves a good trade-off between model accuracy and applicability. Only VT-CPFM-1 is utilized to develop

the model in this study given that VT-CPFM-2 requires additional gear data which is typically not available. The VT-CPFM-1 framework is expressed in Eq.(3):

$$\mathbf{FC} = \begin{cases} \boldsymbol{\alpha_0} + \boldsymbol{\alpha_1 P(t)} + \boldsymbol{\alpha_2 P(t)^2}, & \forall \boldsymbol{P(t) \geq 0} \\ \boldsymbol{\alpha_0}, & \forall \boldsymbol{P(t) < 0} \end{cases} \quad (\mathbf{3})$$

Here FC(t) is the fuel consumption rate at instant t [l/s]; $\boldsymbol{\alpha_0}$, $\boldsymbol{\alpha_1}$ and $\boldsymbol{\alpha_2}$ are the vehicle specific model coefficients that remain to be calibrated, as demonstrated by Eq. (4, 5, 6).

$$\boldsymbol{\alpha_0} = \frac{\boldsymbol{P_{fmp}\omega_{idle}d}}{\boldsymbol{22164(HV)N}} \quad (\mathbf{4})$$

$$\alpha_2 = \frac{\left(F_{city} - F_{hwy}\frac{P_{city}}{P_{hwy}}\right) - \left(T_{city} - T_{hwy}\frac{P_{city}}{P_{hwy}}\right)\alpha_0}{P_{city}^2 - P_{hwy}^2\frac{P_{city}}{P_{hwy}}} \quad (5)$$

$$\boldsymbol{\alpha_1} = \frac{\boldsymbol{F_{hwy} - T_{hwy}\alpha_0 - P_{hwy}^2\alpha_2}}{\boldsymbol{P_{hwy}}} \quad (\mathbf{6})$$

Here P_{fmp} is the idling fuel mean pressure (400,000 *Pa*); d is the engine displacement (*l*); HV is the fuel lower heating value (43,200,000 *J/kg* for diesel fuel and 43,000,000 *J/kg* for gasoline fuel); N is the number of engine cylinders; ω_{idle} is the engine idling speed (*rpm*); F_{city} and F_{hwy} (*l*) are the fuel consumed for the EPA city and highway drive cycles; P_{city}, P_{city}^2, P_{hwy}, P_{hwy}^2 are the sum of the power and power squared over the EPA city- and highway cycle respectively; T_{city} and T_{hwy} are the duration of EPA city and highway drive cycles (s). Most of the parameters typically correspond to either physical characteristics of the vehicles or fuel type, so that they are stated as specifications by the vehicle manufacturers and readily available.

Nonetheless, the fuel economy, used to estimate F_{city} and F_{hwy}, cannot be obtained in this study given that HDVs do not report their fuel economy for standard drive cycles (e.g. the EPA highway and city drive cycles). Consequently, the HDVs model, unlike LDVs, currently cannot be developed using publicly available data; instead, real-world data were gathered.

The VT-CPFM model was extended to modeling HC, CO, NO_x emissions based on the estimated fuel consumption levels. Different model specifications were tested to determine which parameters would be used in the emission model. Stepwise regression analysis was used to determine the mathematical functionality. The final emission modeling framework is illustrated in Eq. (7), in which the square root of the emission is characterized as a polynomial function of speed and fuel consumption, and $\boldsymbol{a, b, c, d, e, f, g, h}$ are model parameters to be calibrated. The square root model guarantees that the emission results will always be positive.

$$\sqrt{\boldsymbol{E(t)}} = \boldsymbol{a + b.v(t) + c.F(t) + d.v(t).F(t) + e.F(t)^2 + f.F(t)^3 + g.v(t).F(t)^2 + h.v(t).F(t)^3} \quad (\mathbf{7})$$

The conventional LDVs emission model had similar formula but more simplified after excluding the speed parameter. Also, future model generalization will be easier by depending on fuel parameter solely. A variety of proposed models underwent calibration and validation procedures before choosing the final model. The models varied between linear,

quadratic, cubic, logarithm and exponential functions. The main intention was to develop an accurate model that does not generate negative emissions. The square root model which is expressed in Eq. (8) was ultimately chosen as the best option to satisfy the criteria and the main objective.

$$\sqrt{E(t)} = constant + a.F(t) + b.F(t)^2 + F(t)^3 \quad (8)$$

Where $F(t)$ is the estimated fuel from VT-CPFM model at time t, $E(t)$ is the CO or HC or NO_x at time t and a, b *and* c are the model regression coefficients.

VT-CPEM modeling framework

The VT-CPEM model is a quasi-steady backward highly-resolved power-based model. Specifically, the inputs required by the model are the following: the instantaneous speed and the vehicle or train characteristics. The outputs of the model are the following: the energy consumption (EC) [kW h/km] by the vehicle for a specific drive cycle, the instantaneous power consumed [kW], and the state of charge (SOC) of the electric battery [%] (for EVs). The modeling approach is illustrated for EVs and ETs respectively.

Electric Vehicle Modeling Approach

The following formulation is used to develop the model for EVs. As this is a backward model, initially, the power at the wheels is computed using Eq. (2). The power at the electric motor ($\mathbf{P_{Electric\ motor}}$) is then computed, given the power at the wheels, considering the driveline efficiency ($\boldsymbol{\eta_{Driveline} = 0.92}$) [2] and, assuming that the efficiency of the electric motor is $\boldsymbol{\eta_{Electric\ motor} = 0.91}$. This is a reasonable assumption according to [26]. Also, in this range, 91% is the value that minimizes the average error between the empirical data and the estimated energy consumption values. While the vehicle is in traction mode the energy flows from the motor to the wheels. In this case the power at the electric motor is higher than the power at the wheels and the power at the wheels is assumed to be positive. Alternatively, in the regenerative braking mode, energy flows from the wheels to the motor. In this case, the power at the electric motor is lower than the power at the wheels and the power is assumed to be negative. While decelerating the electric power is negative and the regenerative braking energy efficiency ($\boldsymbol{\eta_{rb}}$) is computed when $\mathbf{P_{Electric\ motor} < 0}$ using Eq. (9).

$$P_{\text{Electric motor}} < 0 \ \rightarrow P_{\text{Electric motor net}}(t) = P_{\text{Electric motor}}(t) \cdot \eta_{rb}(t) \quad (9)$$

Using this model it is possible also to estimate the final battery state-of-charge (SOC) [%] using Eq. (10) and (11):

$$SOC_{\text{Final}}(t) = SOC_0 - \sum \Delta SOC_i(t) \quad (10)$$

$$\boldsymbol{\Delta SOC_i(t) = SOC_{i-1}(t) - \frac{P_{\text{Electric motor net}}(t)}{3600 \cdot Capacity_{Battery}}} \quad (11)$$

Where $\mathbf{P_{Electric\ motor\ net}(t)}$ is the electric power consumed considering a battery efficiency of $\boldsymbol{\eta_{Battery} = 0.90}$. $\boldsymbol{Capacity_{Battery}}$ is the capacity of the battery in [Wh]. In particular, the

initial SOC is assumed to be $\boldsymbol{SOC_0 = 0.95}$. Given the SOC it is possible to compute the energy consumption (EC) in [kW h/km] using Eq.(12), here d is the distance in [km].

$$\mathrm{EC}\left[\frac{kWh}{km}\right] = \frac{1}{3{,}600{,}000}\int_0^t \mathrm{P}_{\text{Electric motor net}}(t)dt \cdot \frac{1}{d} \tag{12}$$

The instantaneous regenerative efficiency ($\boldsymbol{\eta_{rb}}$) in Eq. (9) can be computed using Eq. (13).

$$\eta_{\mathrm{rb}}(\mathrm{t}) = \begin{cases} \left[e^{\frac{\alpha}{|a(t)^-|}}\right]^{-1}, & \forall a(t) < 0 \\ 0\,, & \forall a(t) \geq 0 \end{cases} \tag{13}$$

Electric Train Modeling Approach

The ETs energy modeling approach is similar to EVs in terms of energy regeneration. Namely, energy is only recovered during braking and the regenerated energy can be estimated using Eq. (13). However, rail trains are powered by either rail power system or catenary instead of in-train battery. Consequently, there is no need to model SOC like EVs. Also, the power function has different model specification compared to EVs, as illustrated in Eq. (14).

$$\mathrm{P_t} = \frac{\left[0.6 + \frac{20}{w_p} + 0.01u_2 + \frac{Ku_2^2}{w_p n_p} + 20\theta + 70\,\frac{u_2^2 - u_1^2}{L}\right] Mu_2}{375} \times 0.746 \tag{14}$$

Where $\mathrm{P_t}$ is the tractive power in [kW], w_p is the weight per railcar axle [tons] consisting of empty railcar weight and total passenger weight (an average of 150 *lbs* is assumed for each passenger in this study), $\mathrm{u_1}$ and $\mathrm{u_2}$ are the instantaneous speed of train [mph], K is train drag coefficient (0.07 as suggested by [32] for the test train in this study), $\mathrm{n_p}$ is the number of axles per rail car, L is distance moved in one second [*ft*], and θ is the positive track gradient (%). As demonstrated by [32], only positive gradient contributes to the grade resistance with an increase of 20 *lbs/ton* per percentage grade. The term $70\,\frac{u_2^2 - u_1^2}{L}$ is the force exerted for acceleration or braking. M is the average weight of the moving train [tons], including the train curb weight and passenger weight.

It should be noted that, in addition to tractive power, the head end power (HEP) should also be included in the total power consumption. Head end power (HEP) is used for train heating, ventilating and air conditioning (HVAC, idling energy consumption (kW)), computed by (maximum HEP per rail car × HVAC operating level × number of rail cars). The HVAC operating level could be assumed to be "normal" level which equals to one-third of maximum HEP.

Data Collection and Preparation

Diesel and Hybrid-Electric Buses

The field data were collected by test driving the buses around the town of Blacksburg, Virginia. The test was conducted on two types of roads: US 460 (highway with a speed limit of 65 mi/h [104 km/h]) and local streets with speed limits ranging between 25 *mi/h* and 45 *mi/h* (40–72 *km/h*) in order to cover a wide range of driving conditions. The test route

comprised a variety of uphill and downhill sections, and thus provided a suitable environment to test different engine load conditions.

A total of 22 transit buses (14 diesel buses and 8 hybrid buses) were tested under similar ambient temperature conditions to minimize the impact of other external factors on the data. Specifically, the diesel buses were classified into four series (19XX, 62XX, 630X, and 632X). The hybrid buses were categorized into two series (601X and 602X). Within the same series, buses have identical vehicle properties, as illustrated in **Error! Reference source not found.** in which the vehicle specification information was provided by Blacksburg Transit.

Table 1: Diesel and Hybrid Bus Information

Bus series number	Model year	Make and model	Length (ft)	Engine model	Horsepower (hp)	Empty weight (lbs.)	Fuel type
19XX	2009	New Flyer SR-1360 D40LFR	40	ISL-07	250-330	28,300	Diesel
62XX	2012	New Flyer SR-1614 XD35	35	ISL-2010	280-330	26,750	Diesel
630X	2013	New Flyer SR-1733 XD35	35	ISL-2010	280-330	26,750	Diesel
632X	2013	New Flyer SR-1734 XD60	60	ISL-2010	280-330	39,675	Diesel
601X	2010	New Flyer Hybrid SR-1439 DE40LFR	40	ISL-07	280	31,140	Hybrid
602X	2010	New Flyer Hybrid SR-1440DE60LFR	60	ISL-07	330	45,860	Hybrid

The Hydraulics + Electrical + Mechanical (HEM) logger was used for data acquisition given its portability and capability of collecting data autonomously without any maintenance. The data were collected from ignition-on to ignition-off, and saved on a microSD card to be uploaded to a server via Wi-Fi. Up to 46 parameters were collected, six of which were employed for the proposed study: time stamp, vehicle speed, fuel consumption rate, latitude, longitude, and altitude. The data were recorded at a frequency of 2 *Hz* or 5 *Hz* and converted to a second-by-second basis. Seventy-five percent of the data set of each bus was taken for calibration and 25% for validation.

The model was calibrated using general linear regression (GLR). Each bus was individually modeled, resulting in an individual parameter set. The parameter sets for all buses in the same series were then averaged to generate a composite (series) model.

Error! Reference source not found. summarizes the parameters needed for model development. Some of the parameters, such as rolling resistance coefficient and driveline efficiency, were obtained from the literature; others were estimated based on the field data. It should be noted that the total mass of the bus is the sum of the vehicle curb weight and passenger load, which is computed as the product of the ridership and the average weight of

an individual passenger. In this study, 179 *lb* (81.5 *kg*) was assumed to be the average passenger weight.

Table 2: Parameters Required for Diesel and Hybrid Bus Model Calibration

Parameters	Value	Data source
Drag coefficient (C_D)	0.78	[27]
Rolling coefficient (C_r)	1.25	[27]
c_1	0.0328	[27]
c_2	4.575	[27]
Driveline efficiency (η)	0.94	[33]
Frontal area (A_f)	6.824 m^2	Blacksburg Transit
Altitude correction factor (C_h)	N/A	Estimated from field data
Vehicle mass (m)	N/A	Estimated from field data
Road grade (G)	N/A	Estimated from field data
Acceleration (a)	N/A	Estimated from field data
Ridership	N/A	Field collection
Speed (v)	N/A	Field collection

CNG Buses

The majority of Los Angeles CNG bus fleet was modeled, as illustrated in Table 3. A total of nine bus series were investigated to cover a wide range of bus characteristics, each of which has the identical vehicle properties.

Table 3: CNG Bus Information

Bus Series Number	Model Year	Engine Make and Model	Bus Empty Weight (lb)	Seating Capacity	Frontal Area (m^2)
3100-3149	2010	Cummins ISL G	29550	25	7.55
5300-5522	2001	DDC Series 50G & Cummins ISL G	28000	40	7.38
5600-6149	2013	Cummins ISL G	30916	38	7.44
7000-7949	2000-2003	DDC Series 50G, Doosan & Cummins ISLG 280	31750	40	7.49
7525-7599	2005	DDC Series 50G	31750	40	7.49
7980-7999	2003	DDC Series 50G	29980	40	7.49
8000-8099	2004-2005	Cummins ISL G	32500	46	7.38
8100-8400	2008-2010	Cummins ISL G	32840	46	9.16
9200-9594	2005-2008	Cummins L Gas Plus and ISLG	47970	57	9.5

MOVES fuel consumption data were used for the VT-CPFM model calibration given a lack of in-field fuel consumption measurements for specific CNG bus models. The fuel consumption data were refined based on fuel type, engine categorization, vehicle classification

and vehicle model year for each bus series. Coupling with the trajectory data collected in Blacksburg, VA (collection procedure see "*Diesel and Hybrid-Electric Buses*"), the model was individually calibrated for each series.

Table 4 summarizes the parameters needed for model development. Some of the parameters, such as rolling resistance coefficient and driveline efficiency, were obtained from the literature; others were either estimated based on the field data or provided by transit agency.

Table 4: Parameters Required for CNG Bus Model Calibration

Parameter	Value	Source
Drag coefficient (C_d)	0.78	[27]
Altitude correction factor (C_h)	N/A[a]	Computed from field data
Vehicle frontal area (A_f)	N/A[a]	Los Angeles Transit agency
Vehicle speed (v)	N/A[a]	Measured in field
Mass (m)	N/A[a]	Los Angeles Transit agency
Rolling coefficient (C_r)	1.25	[27]
c_1	0.0328	[27]
c_2	4.575	[27]
Road grade(G)	N/A[a]	Computed from field data
Acceleration (a)	N/A[a]	Computed from field data
Driveline efficiency (η)	0.94	[27]

Heavy Duty Diesel Trucks (HDDTs)

The data used for model development was collected and provided by the University of California (UC) at Riverside. The modeling effort is aimed to test the applicability of the VT-CPFM framework to modeling the HDDTs within diverse vehicle-technology categories. Consequently, the recruited trucks should differ in a wide range of vehicle-specific parameters. To this end, a total of eight trucks were randomly recruited from used vehicle fleets in Southern California within test categories by vehicle model year and engine model/displacement, and a balance between horse power and manufacturers was attempted. The detailed vehicle information is presented in Table 5. For simplicity, the eight vehicles, from the top to the bottom of Table 5 are labeled as HDDT1, HDDT2, HDDT3, HDDT4, HDDT5, HDDT6, HDDT7, HDDT8 in the following sections.

To measure real-world fuel consumption and emission levels more realistically, UC Riverside developed a mobile emissions research laboratory (MERL) that contains all instrumentation that is normally found in a regular vehicle emission laboratory. MERL weighs approximately 45,000 *lbs* and could serve as a truck load, so that it is capable of capturing the transient fuel consumption and emissions of a truck pulling it when the truck is being tested. Further details of MERL can be found in [11, 34]

The HDDT test was conducted, by the Center for Environmental Research and Technology at UC Riverside, on the roadways in California's Coachella Valley involving long, uninterrupted stretches of road, approximately at sea level. All trucks were tested using standard fuel from the same source. The data were recorded at a frequency of 1 *Hz* and a total

of 238,893 seconds of data were gathered with a collection of 8 parameters for each truck, including CO_2, Carbon Monoxide (CO), Hydro Carbon (HC), Oxides of Nitrogen (NOx), velocity, fuel rate, engine speed and elevation. For more details on data collection procedure, the reader is encouraged to read [11].

Table 6 presents the model inputs for calibration work.

The raw fuel consumption rates were in *g/s* and then converted to *l/s* in order to use the VT-CPFM framework to develop the proposed model. Simultaneously, the unit of velocity was converted from *mi/h* to *km/h* for modeling purposes. Through comparing the second-by-second CO_2 emissions with engine control unit (ECU) data (i.e. velocity, fuel rate and engine speed), a time delay was found to exist. Consequently, a time alignment was needed to synchronize the raw data. Since fuel rates have a strong relationship with emissions, they were utilized to determine the value of the required time shift. The proper time shift was determined through a cross-correlation analysis by which the correlation coefficients between CO_2 and fuel data were estimated by a correlation function for a range of lag times. The lag times with the highest correlations were selected as the optimal events. It should be noted that the CO_2 emission data collected for two of the trucks (HDDT 4 and HDDT 5) were invalid due to an error in the emission sensors of MERL during the collection process, and thus the model does not covered these vehicles. The aligned data was smoothed by a moving average filter, and outliers were identified using a cook's distance procedure.

Table 5: Heavy Duty Diesel Truck Vehicle Information

Make/Model	Model Year	Engine Make/Model	Rated Power (hp)	Engine Size (l)	Vehicle Mass (kg)
International/ 9800 SBA	1997	Cummins/M11-330	330	10.8	7182
Freightliner/ D120	1997	DDC/C-60	360/400	12.7	7758
Freightliner/ D120	1997	Cummins/N14	370/435	14	7029
Freightliner/ C-120	1997	Cummins/N14	370/435	14	7623
Freightliner/ C-120	1998	DDC/C-60	370/430	12.7	8028
Freightliner/ FDL 120	1999	DDC/C-60	470	12.7	8118
Freightliner/ FDL 120	1999	DDC/C-60	360	12.7	8118
Freightliner/FLD 120	2001	CAT/C-15	475	14.6	7092

Table 6: Parameters Required for HDDT Model Calibration

Parameter	Value	Source
Drag coefficient (C_d)	0.78	[27]
Altitude correction factor (C_h)	N/A[a]	Computed from field data
Vehicle frontal area (A_f)	10.0 m^2	[27]
Vehicle speed (v)	N/A[a]	Measured in field
Mass (m)	N/A[a]	Measured in field
Rolling coefficient (C_r)	1.25	[27]
c_1	0.0328	[27]
c_2	4.575	[27]
Road grade(G)	N/A[a]	Computed from field data
Acceleration (a)	N/A[a]	Computed from field data
Driveline efficiency (η)	0.94	[27]

Electric Vehicles

The data used for VT-CPEM calibration was based on the regenerative braking energy efficiency (η_{rb}) computed by Gao et al. (2007) [35]. The VT-CPEM estimates were compared against the regenerative efficiency values reported by Gao for five drive cycles, as shown in the second column of Table 7. The model parameter (α) in Eq. (11) was optimized to minimize the square error between model estimates and Gao's reported values.

Table 7: **Average empirical regenerative braking energy efficiencies [52], modeled average regenerative braking energy efficiencies and corresponding errors.**

	$\hat{\eta}_{rb}$ [%]	$\bar{\eta}_{rb}$ [%]	ε [%]
FTP75	89.69	81.64	−8.97
LA92	82.95	89.41	7.79
US06	86.55	83.76	−3.22
New York	76.16	83.48	9.61
ECE15	95.75	94.48	−1.33

For validation efforts, the Nissan Leaf EV was tested given that this vehicle has been tested by a few research centers and thus experimental data on the energy consumption of this vehicle are available. The validation effort used data collected by the Joint Research Centre (JRC) of the European Commission [36] and by the DOE's Advanced Vehicle Testing Activity (AVTA) of the Idaho Nation Laboratory (INL). The JRC data are related to the following driving cycles: the New European Driving Cycle (NEDC), the World-wide harmonized Light-duty Test Cycle (WLTC) and the World-wide harmonized Motorcycle

emission Test Cycle (WLMC). The New European Driving Cycle (NEDC) for passenger cars is the current legislative cycle used to determine whether a new Light Duty Vehicle (LDV) model meets EU environmental regulations. The United Nations Economic Commission for Europe (UNECE), in an attempt to develop a global test procedure, developed two test cycles, namely: the WLTC for LDVs and the WLMC for two wheelers.

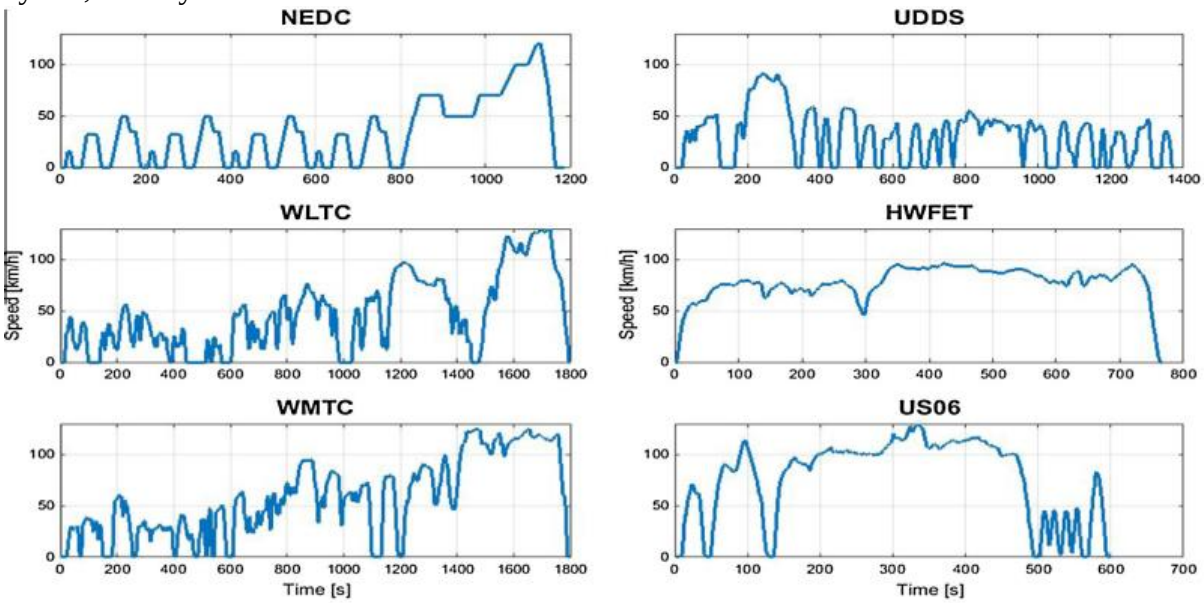

Figure 1: Driving cycles used for model validation

Electric Trains

The data required for calibration were classified into four categories: train information, travel activity data, route characteristics, and the information required to estimate the starting tractive effort. The data were provided by researchers at Georgia Tech who requested the data from the Tri-County Metropolitan Transportation District of Oregon (TriMet), the public agency that operates mass transit in the Portland Metropolitan area. TriMet responded with the information for the Metropolitan Area Express (MAX) Blue Line in Portland. The rolling stock characteristics are illustrated in

Table 8, including the empty weight per rail car, number of axles per rail car, drag coefficient, seating capacity, passenger loading, number of cars per train, and HEP. It should be noted that the trains of the Chicago Brown Line in the table were tested for the model validation purpose. The driving cycle for MAX Blue Line, as illustrated in Figure 2, covers an entire trip of the MAX Blue Line from the starting station to the terminus with a total distance of 32.4 miles. Route characteristics were provided in terms of station name, milepost and elevation in order to generate the grade profile. Basically, the trains, either for MAX Blue Line or Chicago Brown Line, were tested on 115-lb good rails with good cross ties at normal temperature on sunny days. HEP, used for heating, ventilating and air conditioning,

was simplified to three operation levels: normal, high and maximum. Specifically, the normal level operates at a one-third of the maximum load (25 *kW* shown in

Table 8), and the high level functions at two-thirds followed by the maximum level operates at full load.

Table 8: Parameters Required for Electric Train Model Calibration

Parameter	Values	
	MAX blue	Chicago Brown
Weight of empty car (*tons*)	54.5	27.15
Number of axles per car	6	4
Drag coefficient	0.07	0.07
Seating capacity per car	64	49
Percentage loading (peak period)	N/A	87.5
Percentage loading (off-peak period)	N/A	25
Daily percentage loading	43	45
Number of cars per train (peak period)	2	6
Number of cars per train (off-peak period)	2	4
Maximum HEP per car	25	25
HEP operating level	Normal	Normal

The validation data was collected on Brown Line of Chicago rail system. A train on the Chicago subway system was tested by Georgia Tech researchers for the construction of a validation data set. Specifically, the test runs were conducted in the Brown Line to collect second-by-second GPS and position data, resulting in the driving cycle illustrated in Figure 3. The line covers a section of 11.4 mi from the starting station to the terminus. The valid data were gathered on an 8.2 mile section of this route. Likewise, the test was also completed under the same weather and rail conditions as the MAX Blue Line, resulting in the identical bearing, track and weather resistance. The characteristics of the test train are illustrated in Table 8. Compared to the train running on the MAX Blue Line, they have lower railcar weight, seating capacity and the number of axles per car, while higher number of cars per train. It is worth noting that the number of cars per train and passenger load differ between peak and off-peak period, which results in different passenger weights and total train weights at different periods.

The empirical energy used to validate the model was also obtained from the NTD 2011 database, which is the average energy consumption of the Chicago subway system.

The resulting trip-based energy consumption was 36.44 *kWh/VM* and 0.13 *kWh/SM*. Noticeably, the validation effort was made at both levels of *kWh/VM* and *kWh/SM*. Given the different passenger loads and the number of railcars between peak and off-peak periods, the energy consumption was estimated for each period respectively, and the average of the two periods was compared against the empirical measurements. It should be noted that the passenger loads during peak and off-peak periods were computed based on the daily passenger load which can be obtain from NTD database, see [22].

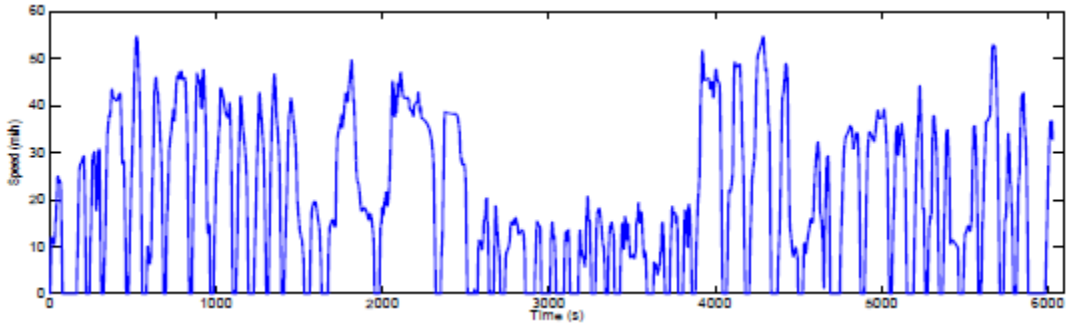

Figure 2: MAX Blue Line Driving Cycle

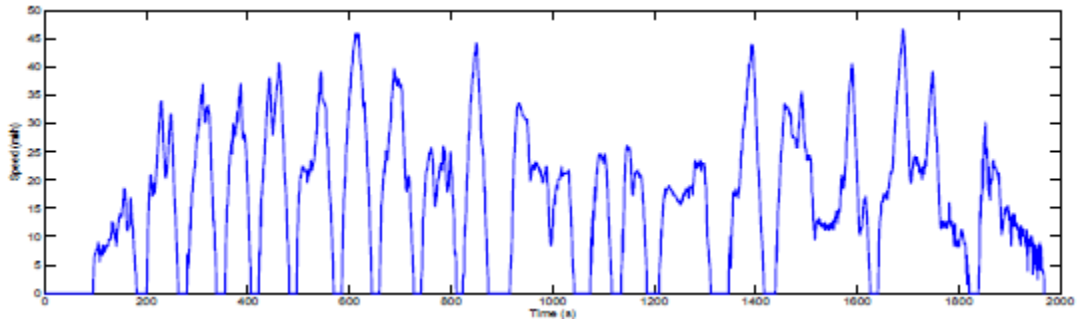

Figure 3: Chicago Brown Line Driving Cycle

Light Duty Vehicles (LDVs)

The emission models were generated from the regression analysis of data from nine normally emitting vehicles. Data were collected at Oak Ridge National Laboratory (ORNL) from six LDVs and three LDTs. Table 9 represents these vehicles in terms of engine displacement, vehicle curb weight, and vehicle type [34]. In addition, the average engine size was 3.1 *l*, the average number of cylinders was 5.6, and the average curb weight was 3,219 *lbs* (1,460 *kg*) [34].

The data were gathered from the tested vehicles driven in the field in two opposite directions on the same road, in order to verify their maximum operating boundaries and minimize the grade and wind effects if they were present. Moreover, the testing was never performed under windy, rainy, or snowy conditions [34].

A chassis dynamometer was used to model the vehicle loadings for the measurement of vehicle emission rates for each vehicle in the laboratory within the attainable speed and acceleration range of each vehicle [34]. The gathered emission data were hydrocarbon (HC),

carbon monoxide (CO) and oxides of nitrogen (NO_x). Data sets of speed, acceleration, emission rates, and fuel consumption were generated.

For each vehicle there were between 1,300 and 1,600 individual measurements, where vehicle speeds ranged from 0-121 *km/h* (0 to 110 *ft/s*) at increments of 1 *km/h*, and vehicle acceleration measurements ranged from -1.5 to 3.7 m/s^2 (-5 to 12 ft/s^2) at increments of 0.3 m/s^2. Emissions *g/s* (*mg/s*) and fuel consumption *l/s* (*gal/h*) for each acceleration and speed measurement were also collected [35].

Table 9: ORNL Test Vehicle Characteristics

Year	Make/Model	Engine PFI= Port Fuel Injection TBI= Throttle Body Injection	Transmission M= Manual, L= Automatic with Lockup	Curb Weight kg
1988	Chevrolet Corsica	2.8 L pushrod V6, PFI	M5	1209
1994	Oldsmobile Cutlass Supreme	3.4 L DOHC V6, PFI	L4	1492
1994	Oldsmobile Eighty Eight	3.8 L pushrod V6, PFI	L4	1524
1995	Geo Prizm	1.6 L OHC 14, PFI	L3	1116
1993	Subaru Legacy	2.2 L DOHC flat 4, PFI	L4	1270
1997	Toyota Celica	1.8 L DOHC 14, PFI	L4	1143
1994	Mercury Villager Van	3.0 L pushrod V6, PFI	L4	1823
1994	Jeep Grand Cherokee	4.0 L pushrod 16, PFI	L4	1733
1994	Chevrolet Silverado	5.7 L pushrod V8, TBI	L4	1823

The ORNL data underwent calibration and validation procedures via the k-fold cross validation method. The k-fold cross validation method divides the dataset into k subsets. At each iteration, one of the k subsets serves as the test set and the rest of the subsets execute the training procedure. This method was applied to CO, HC and NO_x data for each vehicle where the average coefficients and coefficient of determination were calculated.

The estimated fuel consumption results from VT-CPFM were first tested against the measured fuel to find the coefficient of determination. Subsequently, the instantaneous estimated fuel consumption result was introduced in each model as the main parameter.

The resulting slope and R^2 for each vehicle were generated from linear regression between measured fuel and estimated fuel, as illustrated in Table 10. All the vehicles had very good fit, with R^2 above 0.9. The predicted emission levels were processed by utilizing the estimated fuel from the VT-CPFM model after the calibration for each vehicle.

Table 10: Results of Estimated Fuel from VT-CPFM

Make/Model	Slope	R^2

Chevrolet Corsica	1.2	0.95
Oldsmobile Cutlass Supreme	0.92	0.93
Oldsmobile Eighty Eight	1.2	0.91
Geo Prizm	1.4	0.89
Subaru Legacy	1.32	0.9
Toyota Celica	1.2	0.95
Mercury Villager Van	1.29	0.9
Jeep Grand Cherokee	1.5	0.94
Chevrolet Silverado	1.6	0.95

RESEARCH FINDINGS

Diesel and Hybrid Buses

The resulting models are illustrated in Table 11Table 11. The impact of road grade and vehicle load on the estimated fuel consumption as it varies with cruise speed, has been analyzed. As demonstrated by **Error! Reference source not found.**, the model, in general, represents fuel consumption as a bowl-shaped function of vehicle speed at non-negative grade levels, suggesting that optimum cruise speeds are achieved within the lower bound and upper bound of the speed range. Specifically, **Error! Reference source not found.** characterizes the optimum cruise speed as it varies with road grade, demonstrating that higher uphill grades result in a lower optimum cruise speed, whereas steeper downhill roads require a higher cruise speed to minimize fuel consumption level (which is not recommended for safety purposes). **Error! Reference source not found.** summarizes the impact of vehicle load on the optimum cruise speed. Basically, heavier vehicles accrue lower optimum speeds when moving uphill and higher when moving downhill. It is worth noting that, as demonstrated by **Error! Reference source not found.**b, the optimum speeds remain constant with an increase in vehicle weight when the road grade is −4%, −6% and −8%. This is attributed to the fact that the analysis is performed only for the speed range of 0–100 *km/h*, and, at these grade levels, the optimum speeds reach the maximum level at a low vehicle load. In addition, the optimum speeds are demonstrated by **Error! Reference source not found.**a (uphill) to be more sensitive to vehicle load at higher grade levels.

Table 11: Diesel and Hybrid Bus Fuel Consumption Models

Bus series number	α_0	α_1	α_2
19XX	1.66E-03	8.68 E-05	1.00E-08
62XX	1.13E-03	5.69 E-05	1.00E-08
630X	9.76E-04	6.44 E-05	1.00E-08
632X	1.41E-03	8.21 E-05	1.00E-08
601X	1.00E-03	5.18 E-05	1.00E-08

602X	1.38E-03	6.22 E-05	1.00E-08

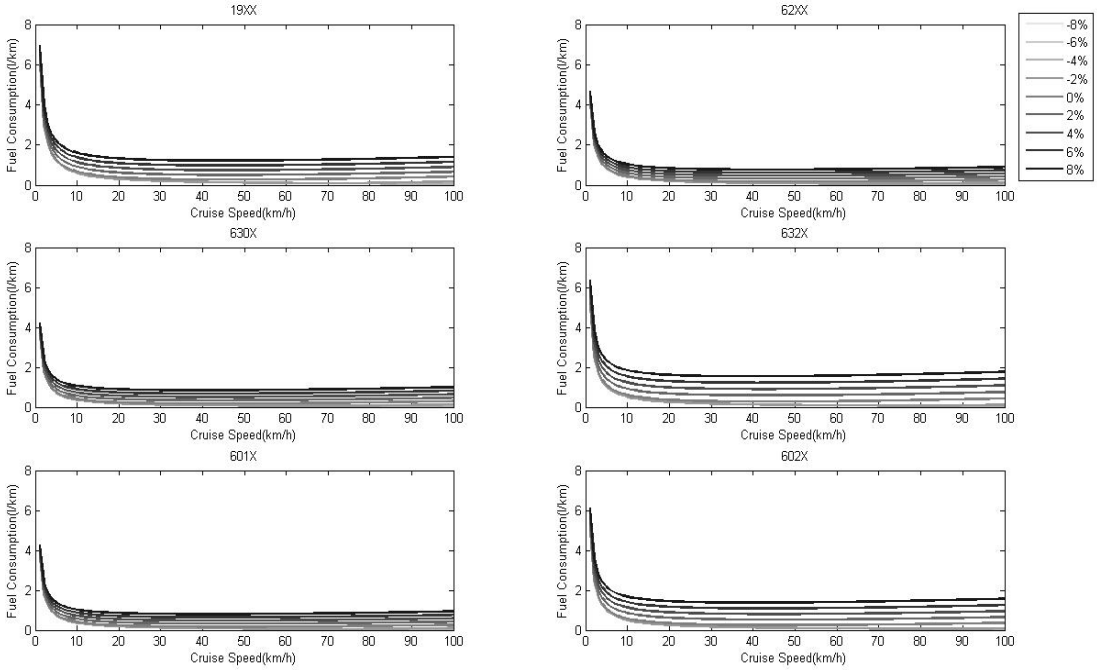

Figure 4: Fuel consumption vs. cruise speed at different grades (diesel and hybrid buses)

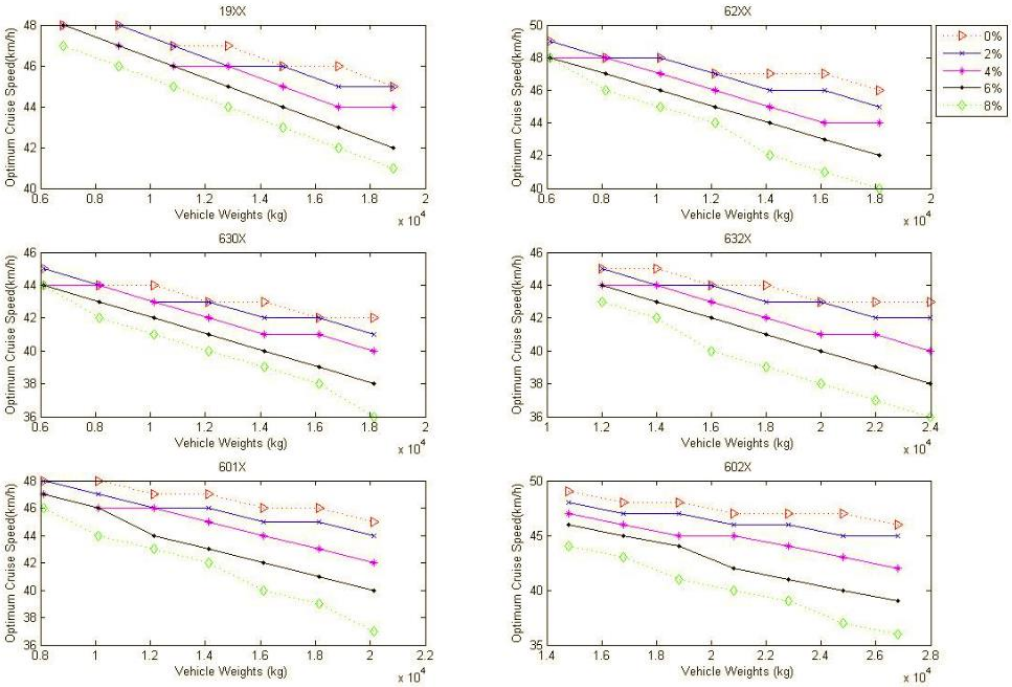

(a)

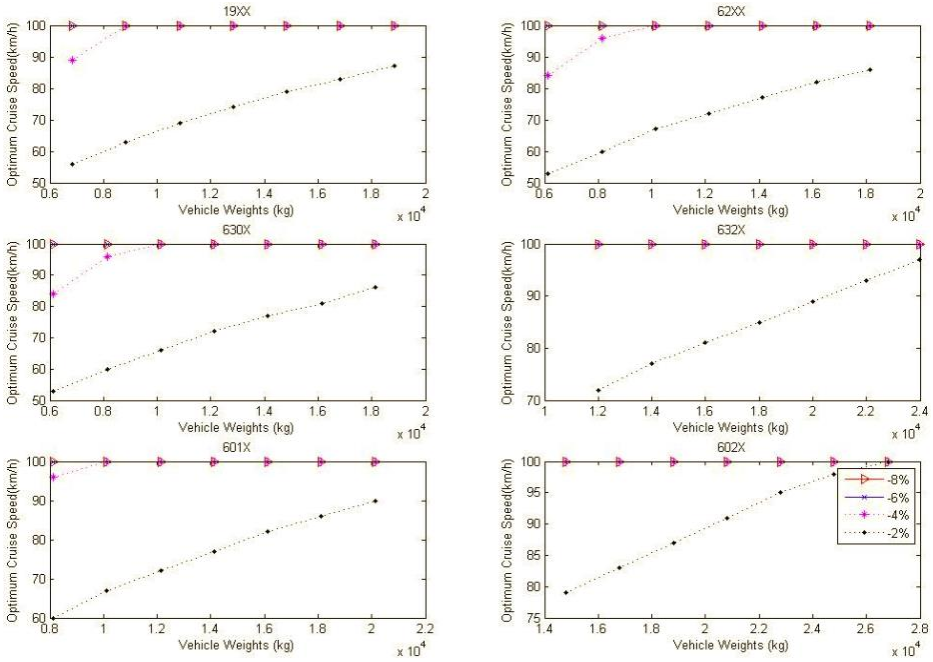

(b)

Figure 5: Impact of vehicle weight on optimum fuel economy cruise speed at different grade levels (diesel and hybrid buses): (a) uphill; (b) downhill.

The developed model's estimates for each series were compared against the field measurements of a real bus in that series as well as the predictions from CMEM and MOVES. Furthermore, the variation of fuel consumption with cruise speed was tested and compared with that of CMEM.

As summarized in Table 12**Error! Reference source not found.**, VT-CPFM and CMEM can generate approximately accurate estimates by having proximate coefficient of determination (R^2); however, CMEM produces a bang-bang type of control. MOVES produces the least accurate estimates given that it is designed for conformity use instead of instantaneous analysis. Furthermore, the slopes of the regression lines of model estimates versus field measurements demonstrate that VT-CPFM and CMEM, in general, underestimate fuel consumption levels, while VT-CPFM can provide better estimates by having higher slope values. MOVES generates an underestimate for some series while overestimating for others, which is explained by the fact that the buses employed by the MOVES database are a composite of numerous bus categories rather than the specific type used in this study.

Table 12: Diesel and Hybrid Bus Model Validation

Bus series No.	Convex (VT-CPFM): R^2	Convex (VT-CPFM): Slope	Concave (VT-CPFM): R^2	Concave (VT-CPFM): Slope	CMEM: R^2	CMEM: Slope	MOVES: R^2	MOVES: Slope

19XX	0.81	0.78	0.82	0.81	0.81	0.66	0.74	0.82
62XX	0.78	0.77	0.80	0.88	0.80	0.76	0.74	1.20
630X	0.75	0.83	0.76	0.75	0.72	0.73	0.68	1.06
632X	0.79	0.80	0.80	0.85	0.80	0.69	0.70	0.60
601X	0.63	0.79	0.63	0.75	0.63	0.67	0.57	1.13
602X	0.69	0.90	0.69	0.90	0.70	0.82	0.67	0.76

In validating the model, a comparison was made to CMEM, as demonstrated in Figure 6, which gives two example results. The proposed model generates an optimum cruise speed consistent with CMEM and produces the same bowl-shaped curve as a function of cruise speed. Specifically, the optimum cruise speed ranges between 39 and 47 *km/h* for all of the tested buses for grades varying from 0% to 8% (lower than LDVs: 60–80 *km/h*), and decreases with the rise of grade and vehicle load.

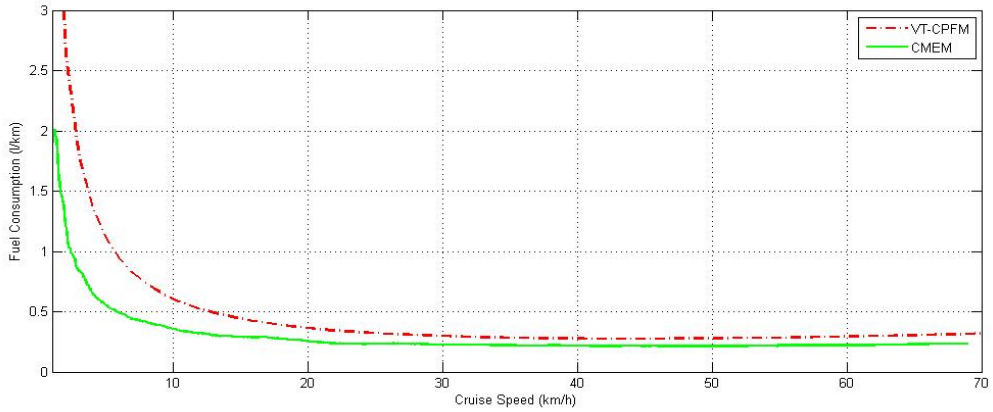

(a)

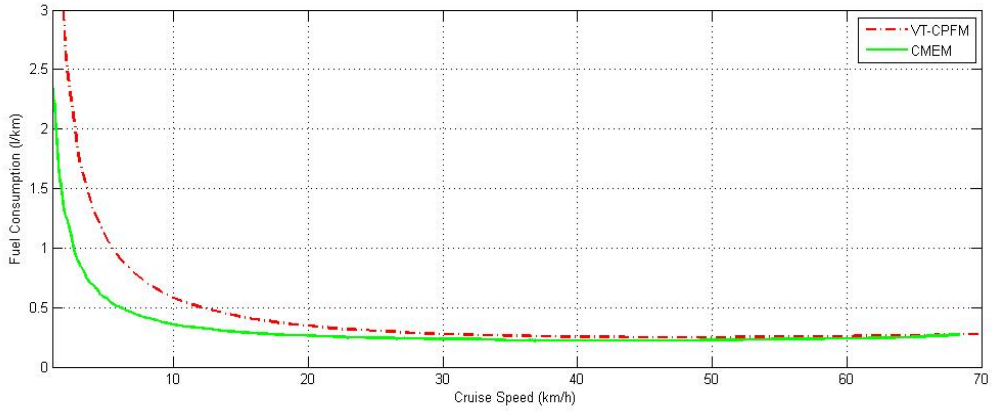

(b)

Figure 6: Fuel consumption varying with cruise speed, VT-CPFM vs. CMEM: (a) diesel bus (632X); (b) hybrid bus (602X).

CNG Buses

The resulting models are illustrated in Table 13**.** The sensitivity of model estimates to road grade and vehicle load has been analyzed. The example results were presented in **Error! Reference source not found.** and For the validation purpose, the trajectory data independent of calibration dataset was used. The model estimates were instantaneously compared against the MOVES fuel consumption. As illustrated in Figure 9, the VT-CPFM model can predict fuel consumption consistent with MOVES measurements by following the peaks and valleys of the data. Statistically, the models produce R^2 values of 0.85 for most of the bus series, demonstrating a good model fit.

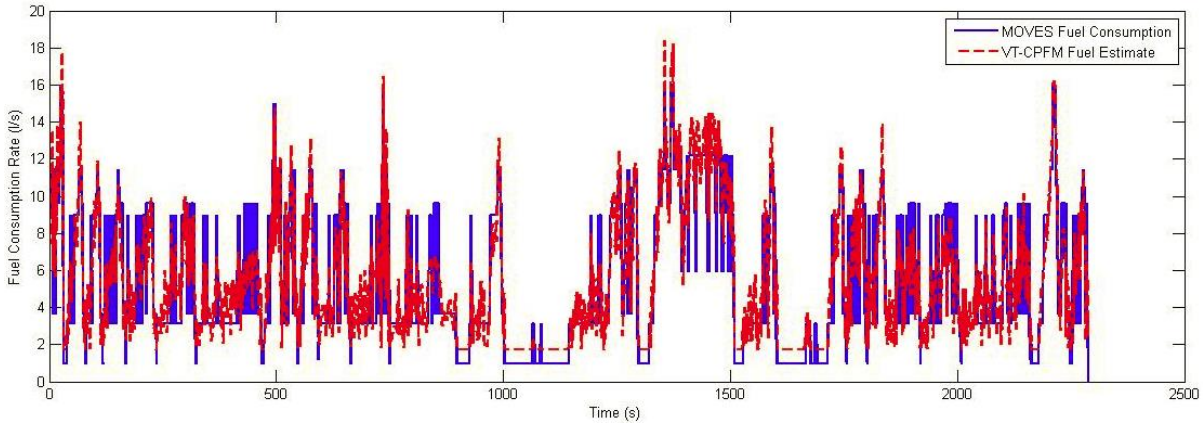

Figure 9: Instantaneous CNG bus model validation

Furthermore, fuel consumption varying with cruise speed was also tested and compared with MOVES. As demonstrated by Figure 10, the example result indicates that the proposed model produces the consistent bowl-shaped curve as a function of cruise speed. Specifically, the optimum cruise speed ranges between 39 and 46 *km/h* for all of the tested bus series varying grades from 0% to 8%, which is similar to conventional and hybrid buses.

. Specifically, the model, similar to conventional and hybrid buses, represents fuel consumption as a bowl-shaped function of vehicle speed at non-negative grade levels, suggesting that optimum cruise speeds are achieved within the lower bound and upper bound of the speed range. For the validation purpose, the trajectory data independent of calibration dataset was used. The model estimates were instantaneously compared against the MOVES fuel consumption. As illustrated in Figure 9, the VT-CPFM model can predict fuel consumption consistent with MOVES measurements by following the peaks and valleys of the data. Statistically, the models produce R^2 values of 0.85 for most of the bus series, demonstrating a good model fit.

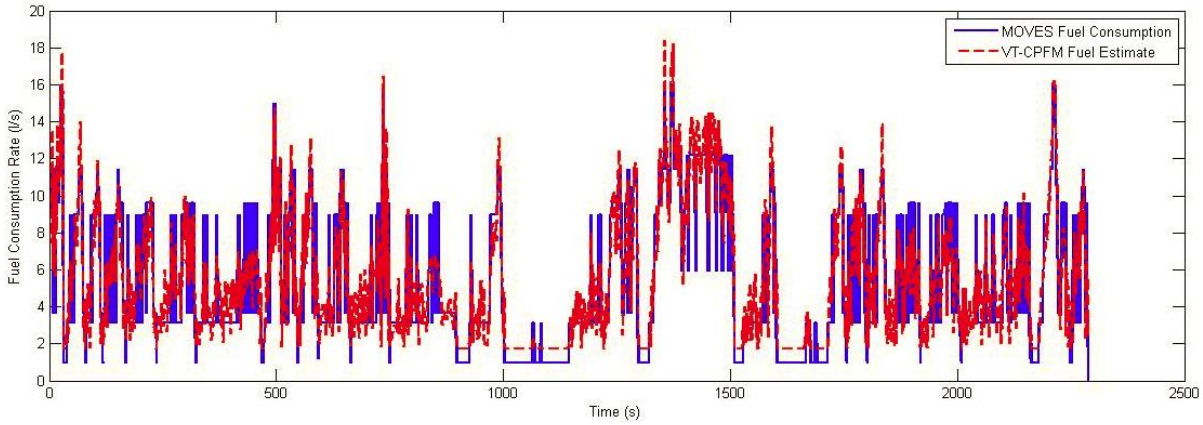

Figure 9: Instantaneous CNG bus model validation

Furthermore, fuel consumption varying with cruise speed was also tested and compared with MOVES. As demonstrated by Figure 10, the example result indicates that the proposed model produces the consistent bowl-shaped curve as a function of cruise speed. Specifically, the optimum cruise speed ranges between 39 and 46 *km/h* for all of the tested bus series varying grades from 0% to 8%, which is similar to conventional and hybrid buses. summarizes the impact of vehicle load on the optimum cruise speed. Basically, heavier vehicles accrue lower optimum speeds when moving uphill and higher when moving downhill. Also, for a given vehicle load, steeper roads result in lower optimum cruise speed.

Table 13: CNG Bus Fuel Consumption Model

Bus Series Number	α_0	α_1	α_2
3100-3149	1.729	1.08E-01	1.00E-05
5300-5522	2.058	1.36E-01	1.00E-05
5600-6149	1.718	1.04E-01	1.00E-05
7000-7949	2.046	1.21E-01	1.00E-05
7525-7599	1.716	1.01E-01	1.00E-05
7980-7999	1.728	1.07E-01	1.00E-05
8000-8099	1.724	9.86E-02	1.00E-05
8100-8400	1.725	9.70E-02	1.00E-05
9200-9594	1.728	6.71E-02	1.00E-05

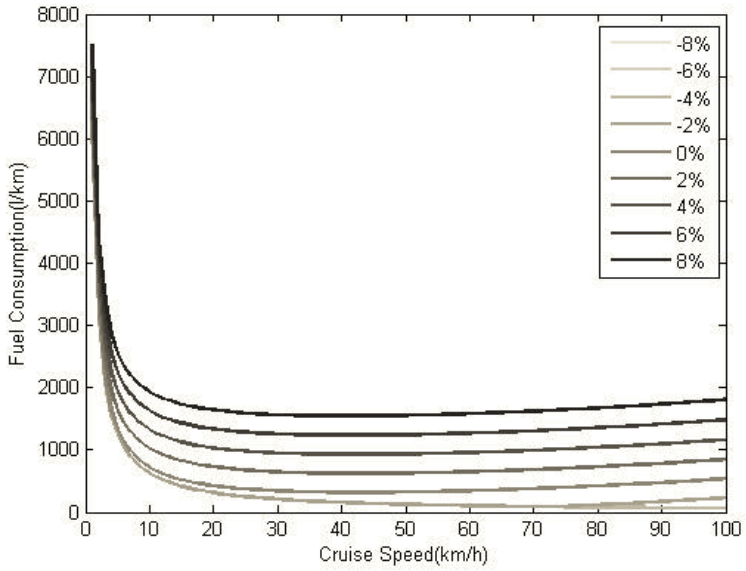

Figure 7: Fuel consumption vs. cruise speed at different grades (CNG bus)

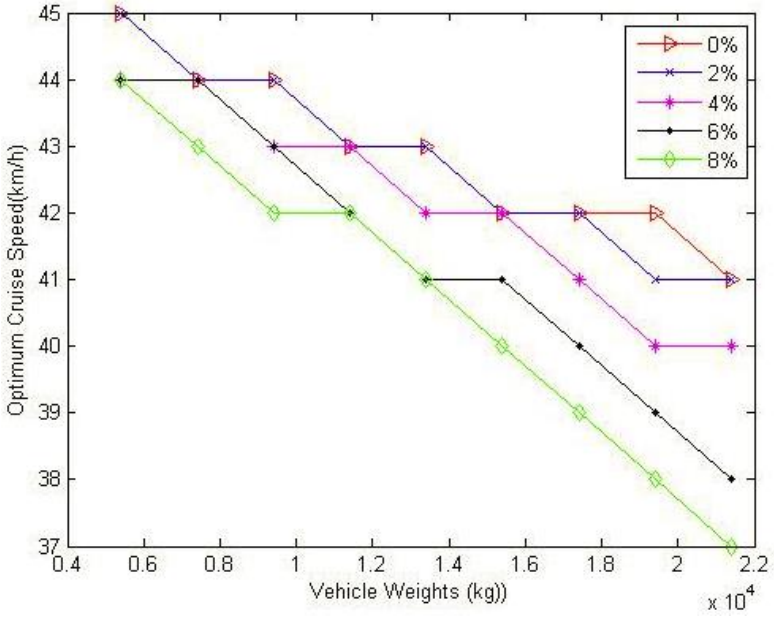

Figure 8: Impact of vehicle weight on optimum fuel economy cruise speed at different grade levels (CNG bus)

For the validation purpose, the trajectory data independent of calibration dataset was used. The model estimates were instantaneously compared against the MOVES fuel consumption. As illustrated in Figure 9, the VT-CPFM model can predict fuel consumption consistent with MOVES measurements by following the peaks and valleys of the data. Statistically, the models produce R^2 values of 0.85 for most of the bus series, demonstrating a good model fit.

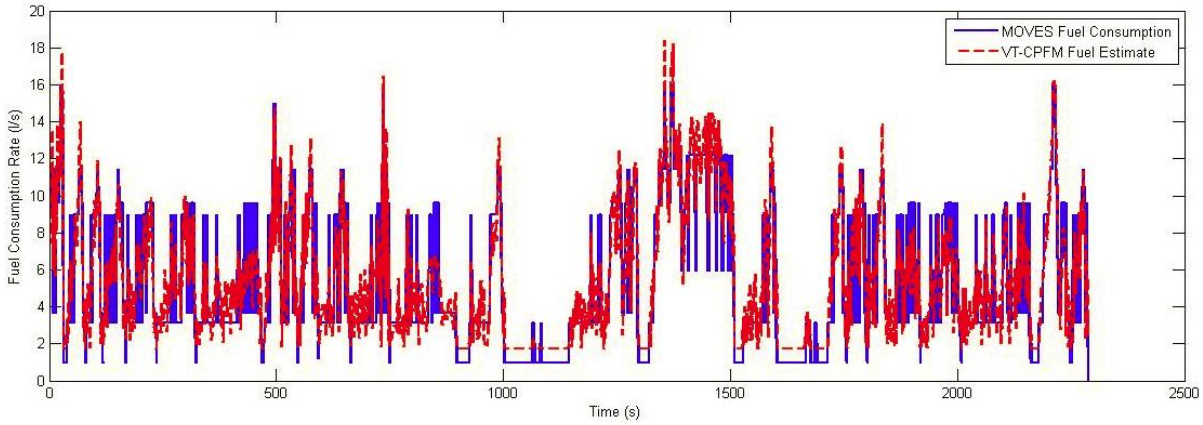

Figure 9: Instantaneous CNG bus model validation

Furthermore, fuel consumption varying with cruise speed was also tested and compared with MOVES. As demonstrated by Figure 10, the example result indicates that the proposed model produces the consistent bowl-shaped curve as a function of cruise speed. Specifically, the optimum cruise speed ranges between 39 and 46 *km/h* for all of the tested bus series varying grades from 0% to 8%, which is similar to conventional and hybrid buses.

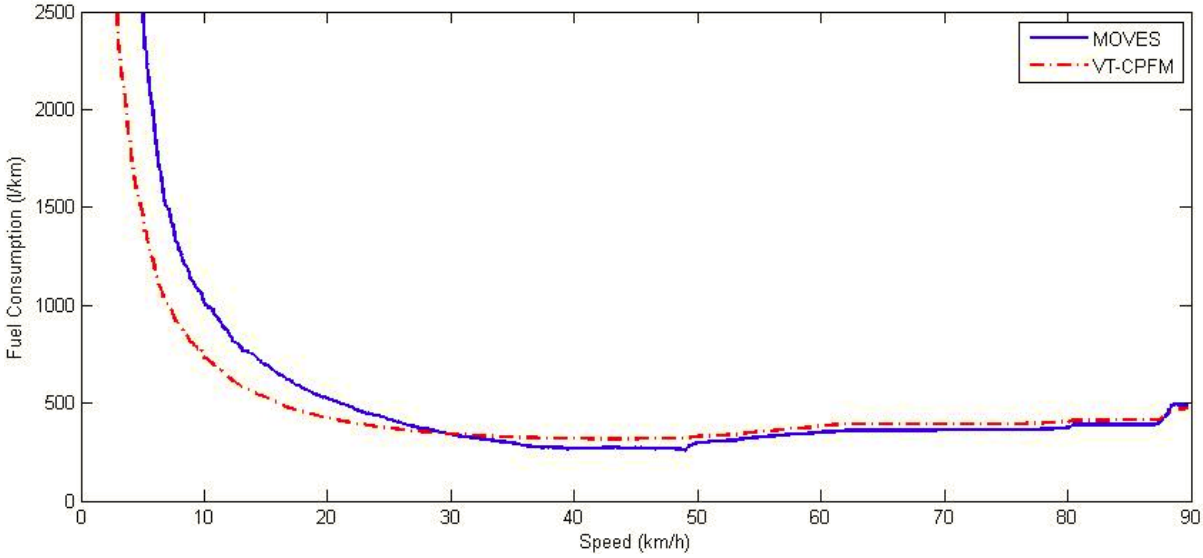

Figure 10: Fuel consumption varying with cruise speed, VT-CPFM vs. MOVES.

Heavy Duty Diesel Trucks (HDDTs)

HDDT Fuel Consumption Modeling Results

Each tested truck was individually modeled. The resulting models are illustrated in Table 14. The effects of road grade and vehicle weight on the optimum fuel economy cruise speed were evaluated. As illustrated in Figure 11, the model produces a bowl-shaped curve as a function of cruise speed and higher road grades result in higher fuel consumption levels, which is similar to LDVs and buses.

Heavier vehicles, as demonstrated in Figure 12, have higher optimum cruise speeds when moving downhill while lower when moving uphill. It should be noted that, in Figure 12a, optimum cruise speeds remain constant with an increase in vehicle weight when the road grade is -8%, -6% and -4%. This is because the sensitivity analysis was performed only for the speed range of 0-100 *km/h* and the optimum cruise speeds already reached the maximum level when vehicle weights were at a low level (e.g. 17,000 *kg*). Furthermore, Figure 12b clearly indicates that the optimum cruise speeds are more sensitive to vehicle weight at higher grade levels.

Table 14: HDDT Fuel Consumption Models

Truck classification	α_0	α_1	α_2
HDDT 1	1.56E-03	8.10E-05	1.00E-08
HDDT 2	2.48E-03	7.14E-05	1.00E-08
HDDT 3	2.26E-03	7.82E-05	1.00E-08
HDDT 4	1.80E-03	7.96E-05	1.00E-08
HDDT 5	2.02E-03	7.59E-05	1.00E-08
HDDT 6	1.45E-03	8.48E-05	1.00E-08
HDDT 7	1.31E-03	8.63E-05	1.00E-08
HDDT 8	2.16E-03	7.98E-05	1.00E-08

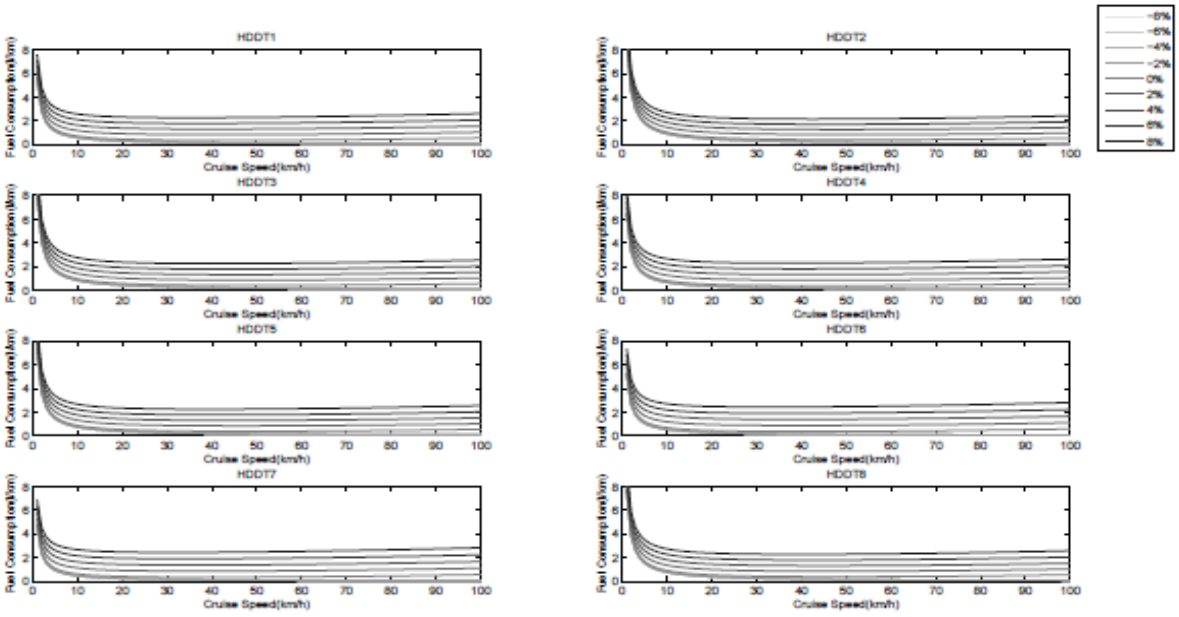

Figure 11: HDDT Fuel consumption vs. cruise speed at different grades

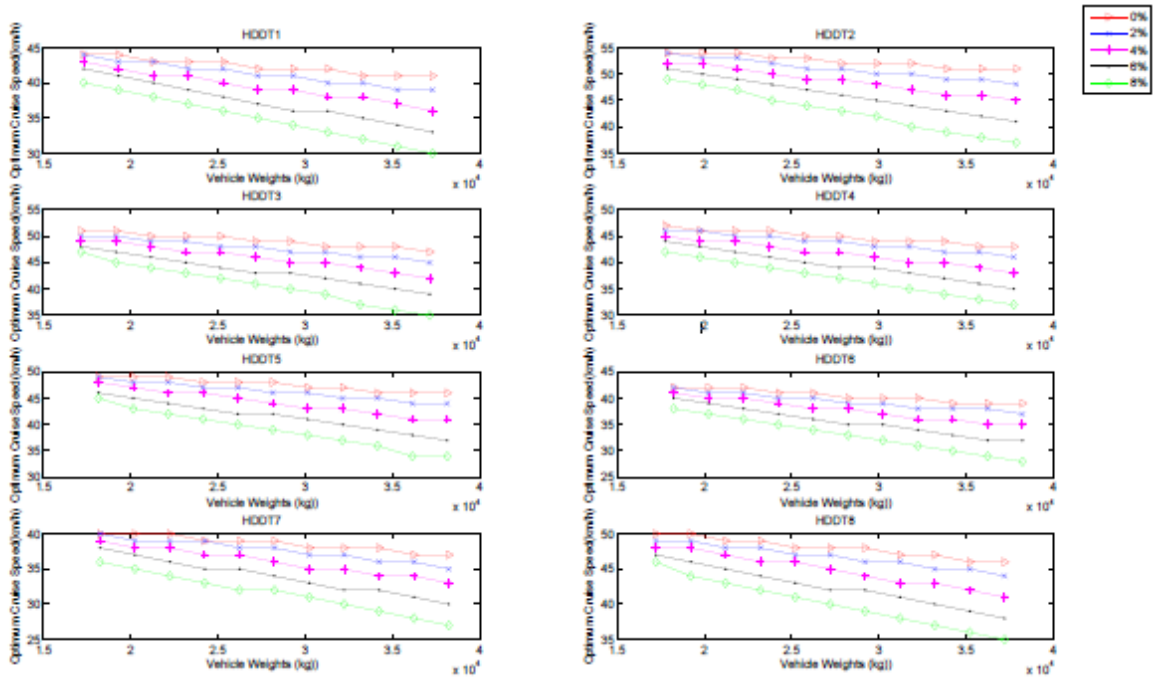

(a)

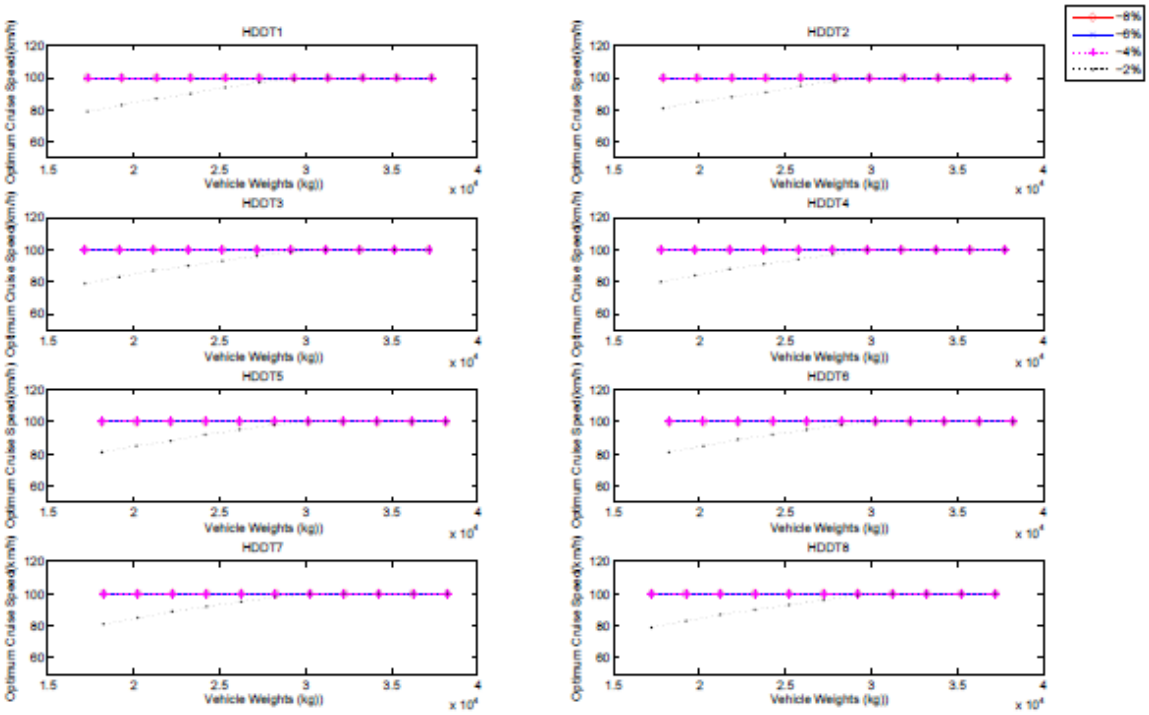

(b)

Figure 12: Impacts of vehicle weight on the optimum fuel economy cruise speed at different grade levels (HDDT)

12

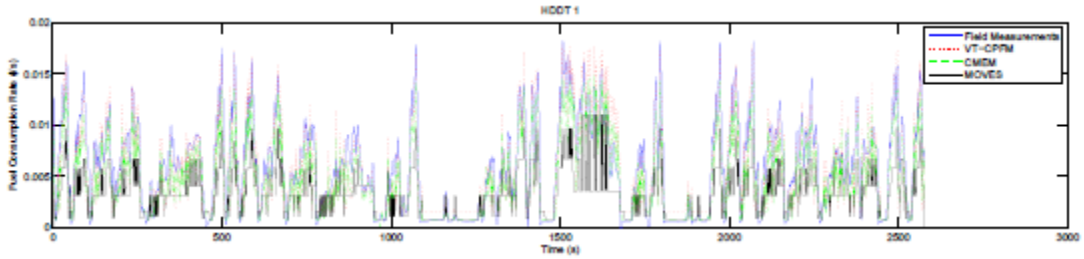

(a) HDDT 1

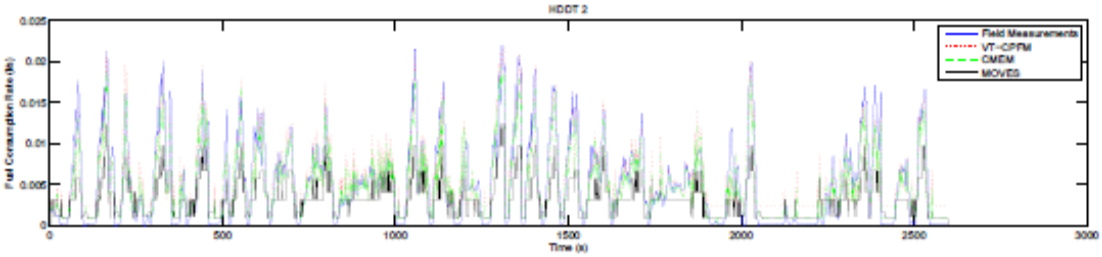

(b) HDDT 2

Figure 13: HDDT model validation

Table 15: HDDT Model Validation

Truck Type	VT-CPFM (concave)		VT-CPFM (convex)		CMEM		MOVES	
	R^2	Slope	R^2	Slope	R^2	Slope	R^2	Slope
HDDT1	0.82	0.93	0.8	0.87	0.87	0.78	0.72	0.42
HDDT2	0.83	0.81	0.81	0.76	0.87	0.75	0.76	0.39
HDDT3	0.84	0.92	0.83	0.81	0.9	0.78	0.77	0.42
HDDT4	0.87	0.91	0.86	0.88	0.9	0.77	0.78	0.42
HDDT5	0.66	0.75	0.64	0.69	0.71	0.65	0.57	0.39
HDDT6	0.78	0.89	0.77	0.86	0.83	0.72	0.72	0.38
HDDT7	0.81	0.82	0.81	0.78	0.85	0.64	0.74	0.35
HDDT8	0.84	0.86	0.84	0.84	0.89	0.79	0.78	0.43

In validating the proposed model, the variation of fuel predictions over cruise speed was compared against CMEM estimates, as illustrated in Figure 14 which gives one example result. The two models have highly consistent bowl shaped curves as a function of cruise speed, demonstrating that the proposed model can produce robust fuel estimates. Specifically, the optimum cruise speed ranges between 32-52 *km/h* (lower than LDVs: 60-80 *km/h*) for all of the test trucks varying the grade level from 0% to 8%, and moves towards the negative direction with the increase of vehicle load and grade level as demonstrated by Figure 12a.

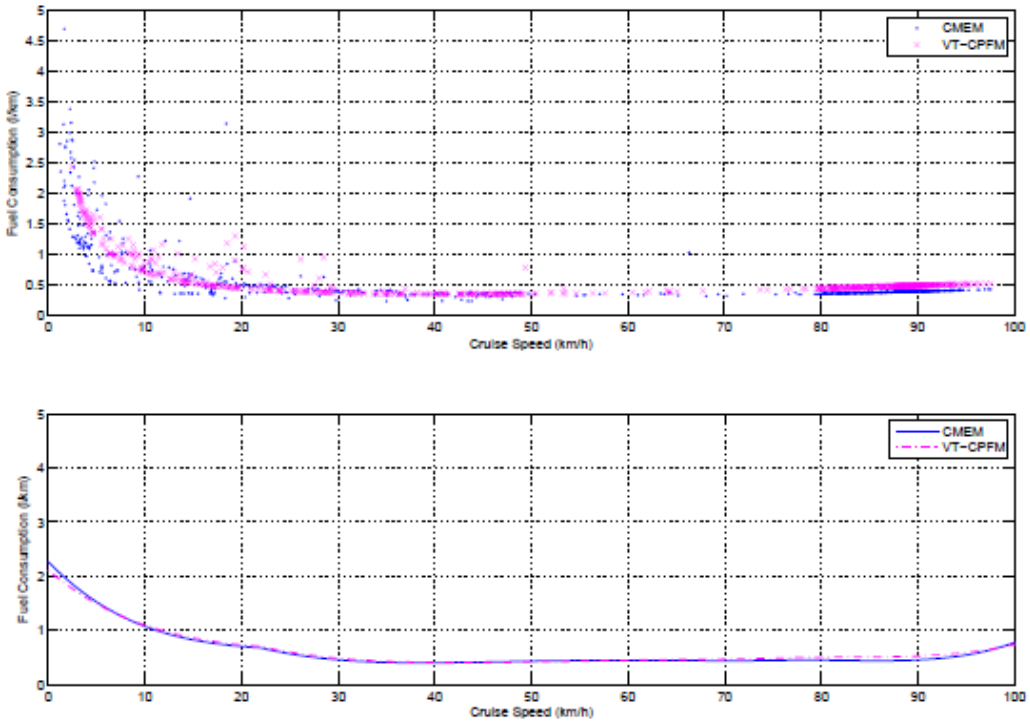

Figure 14: HDDT model impact of cruise speed on fuel consumption levels: VT-CPFM vs. CMEM

CO_2 can be estimated from the carbon balance equation using the fuel consumption, HC and CO estimates. Given that the magnitude of CO_2 emissions is significantly higher than HC and CO emissions, the fuel consumption level is thus the primary factor that affects CO_2 emissions. As demonstrated in [2], CO_2 emission is linearly related to fuel consumption. Eq.(15) was used to capture the relationship between CO_2 and fuel predictions. The model was firstly calibrated for each truck with CO_2 in *g/s* and fuel consumption in *l/s*, and the values of θ were then averaged over individual models to generate the average model given that the relationship between CO_2 and fuel consumption is only related to fuel type rather than vehicle type. The value of 2070 was used to compute CO_2 emissions from fuel consumption estimates. It is found that model estimates are in general consistent with field measurements, as the example results illustrated in Figure 15. The results of other validation efforts are summarized in Table 16 which has an R^2 values ranging between 0.74 and 0.85. In general, the model provides reliable CO_2 predictions. Noticeably, the model cannot be validated for HDDT 4 and HDDT 5 due to a lack of valid CO_2 field measurements, and the model performance is thus not discussed for these vehicles.

$$\boldsymbol{\theta = \frac{CO_2(t)}{FC(t)}} \qquad \textbf{(15)}$$

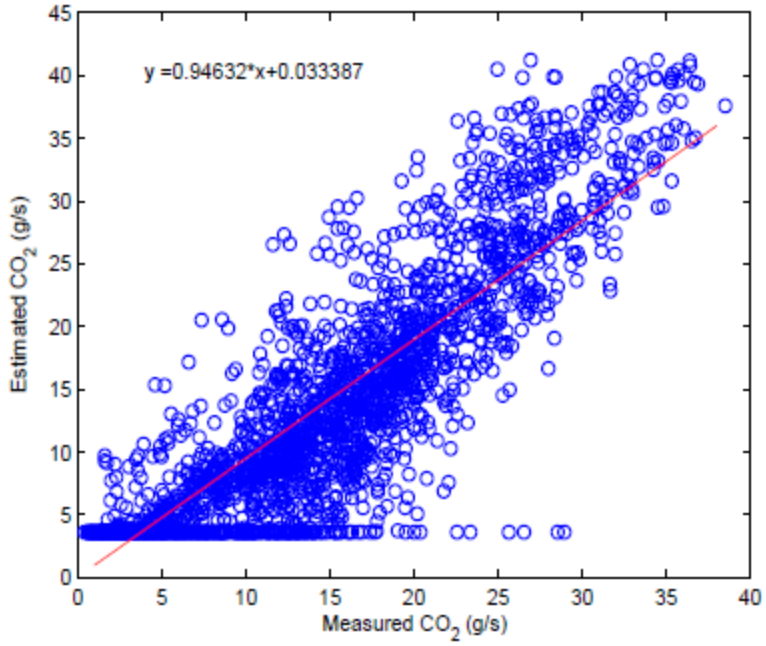

Figure 15: CO_2 estimation using fuel consumption model (HDDT 1)

Table 16: CO_2 Emission Model Validation

Truck Classification	Coefficients of determination (R^2)	Slope
HDDT 1	0.78	0.95
HDDT 2	0.85	0.72
HDDT 3	0.81	0.82
HDDT 4	NA	NA
HDDT 5	NA	NA
HDDT 6	0.74	0.73
HDDT 7	0.81	0.65
HDDT 8	0.79	0.82

HDDT Emission Modeling Results

Like fuel consumption modeling, each testing truck was individually modeled for the three types of pollutant emissions HC, CO and NO_x. The sample modeling coefficients are represented in Table 17.

Table 17: HDDT Pollutant Emission Models

Emission	*a*	*B*	*C*	*d*	*e*	*f*	*g*	*h*
CO	-0.023	0.003	58.967	-1.089	-3201.70	70.879	47595	-1209.50
HC	0.035	0.001	11.219	-0.216	-796.41	16.847	22888	-456.31
NO_x	0.049	0.002	100.098	-1.017	-10536.00	161.680	339250	-5640.50

The models were tested using the dataset independent of the calibration data. Due to the space limitation, this report only presents the example results for one truck; namely, HDDT 1. The results are illustrated in Figure 16 to represent the behavior of emissions as a function of VT-CPFM fuel consumption and speed. It is found that emissions increase with the increasing fuel consumption, and the highest emission levels occur at the peak of fuel consumption. NO_x has the highest level of emissions and is the most well-distributed emission compared with CO and HC. NO_x makes up the largest portion of diesel emissions at more than 50% because diesel engines are lean combustion engines and the concentration of CO and HC is minimal [37].

The VT-CPFM emission model maintains consistency using the same model to predict emissions. The accuracy of the model was evaluated by estimating the coefficient of determination (R^2) of CO, HC, and NO_x for the eight trucks. Table 18 shows R^2 values for each truck across the three emissions and the average values for each emission. NO_x has the highest R^2 values, followed by CO then HC, which has the lowest R^2 values. Figure 16 illustrates this by showing the well-distributed data for NO_x, which were measured more easily and captured more accurately than CO and HC for some trucks. Diesel engines emit low levels of HC [37], making it more difficult to predict accurately compared with NO_x. Consequently, NO_x has the highest average R^2 of 0.857, followed by CO then HC (0.749 and 0.582, respectively).

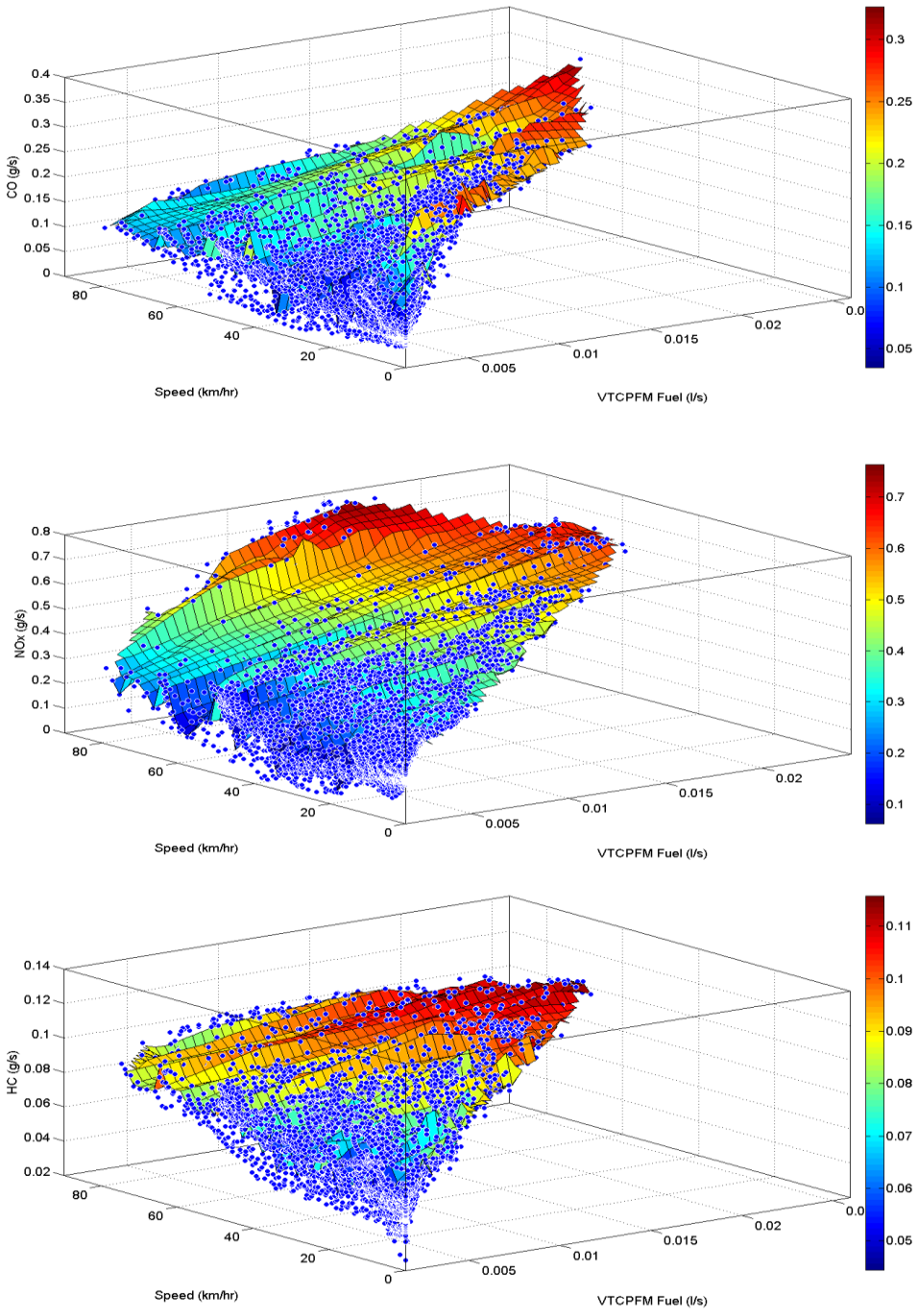

Figure 16: **Sample of the randomized emission data with speed and VT-CPFM fuel consumption (HDDT 1).**

Table 18: HDDT Pollutant Emission Model Validation

Vehicle ID	CO	HC	NO_x
HDDT 1	0.752	0.753	0.898
HDDT 2	0.749	0.226	0.821
HDDT 3	0.710	0.583	0.897
HDDT 4	NA	0.651	0.915
HDDT 5	0.721	0.440	0.676
HDDT 6	0.752	0.796	0.858
HDDT 7	0.739	NA	0.862
HDDT 8	0.821	0.626	0.929
Average	0.749	0.582	0.857

The performance of the VT-CPFM emission model was further evaluated and validated by comparing it with CMEM's results (Table 19). The predicted emission values were plotted against measured field data to fit the regression line to estimate R^2 for each model (Figure 17, Figure 18, Figure 19; Table 19). Table 19 summarizes the individual and average R^2 values, revealing the robustness of the model based on its goodness of fit. It is evident that the average R^2 values of the VT-CPFM emission model are higher than those for the CMEM model, demonstrating the superior performance of the model. In general, the VT-CPFM model has higher R^2 values for almost all the vehicles compared to CMEM.

Table 19: R^2 Values for Emission Field Data vs. Estimates for CMEM and VT-CPFM

Vehicle ID	VT-CPFM (CO)	CMEM (CO)	VT-CPFM (HC)	CMEM (HC)	VT-CPFM (NO_x)	CMEM (NO_x)
HDDT 1	0.728	0.586	0.745	0.695	0.924	0.904
HDDT 2	0.779	0.708	0.172	0.148	0.832	0.820
HDDT 3	0.665	0.487	0.566	0.525	0.925	0.951
HDDT 4	NA	NA	0.658	0.512	0.934	0.938
HDDT 5	0.707	0.594	0.423	0.404	0.700	0.661
HDDT 6	0.789	0.645	0.162	0.107	0.880	0.866
HDDT 7	0.743	0.510	NA	NA	0.896	0.824
HDDT 8	0.836	0.613	0.578	0.392	0.955	0.939
Average	0.750	0.592	0.472	0.397	0.881	0.863

The two models are similar in terms of the order of goodness of fit for NO_x emissions. Table 19 shows that the average coefficient of determination (R^2) NO_x emission values for the two models are the highest. Alternatively, the coefficient of determination is the lowest for HC emission estimates. The values imply that NO_x has the best fit. VT-CPFM has a slightly higher R^2 value than CMEM (0.881 versus 0.863). On the other hand, the average R^2 values for HC demonstrate the relatively poor fit between the predicted and measured field data, which is due to the low HC emission levels as mentioned before. Nevertheless, VT-CPFM has better HC estimates than CMEM as expressed in the average R^2 values (0.472 versus 0.397). Finally, the VT-CPFM model has a relatively average fit of $R^2 = 0.750$ compared to CMEM with a relatively poor fit of $R^2 = 0.592$ for CO emissions.

The VT-CPFM model is simple, with only eight coefficients and two main parameters, speed and fuel. CMEM requires extensive and complicated data to estimate emissions. For instance, CMEM requires engine speed data, which would require installation of onboard diagnostics to measure. On the other hand, the data used by VT-CPFM are publicly available except for the speed data, which can be easily collected using a GPS device.

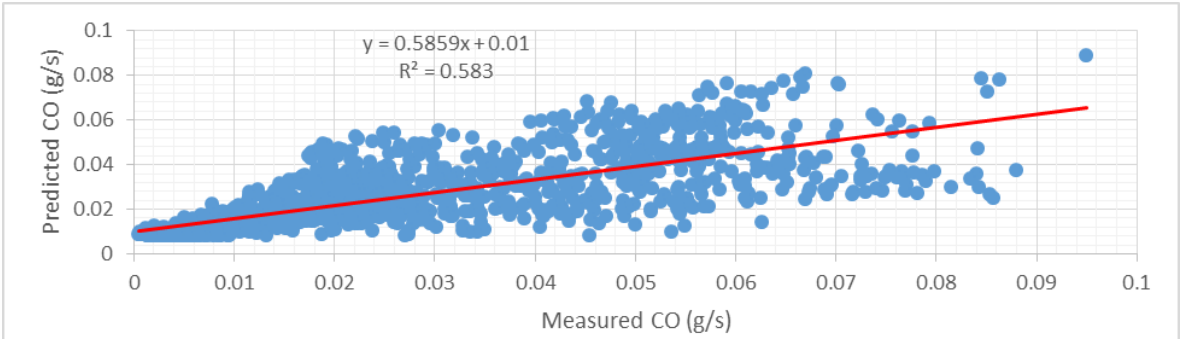

(a) CMEM

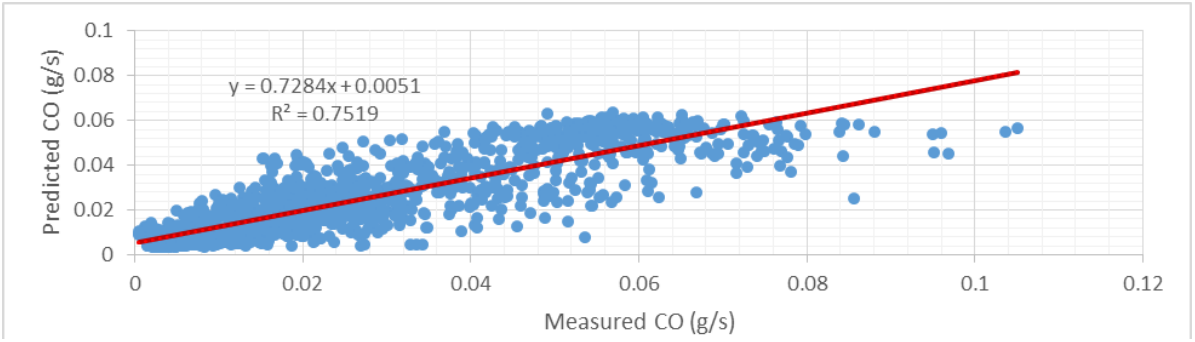

(b) VT-CPFM

Figure 17: Comparison between (a) CMEM and (b) VT-CPFM of CO estimates

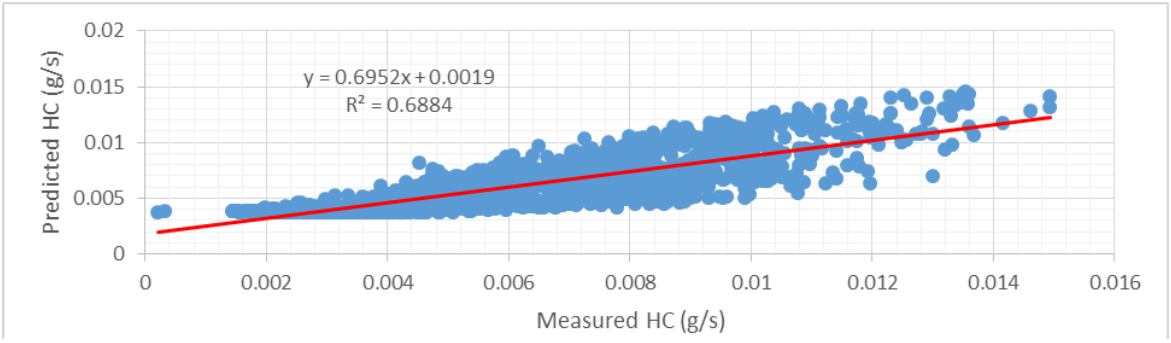

(a) CMEM

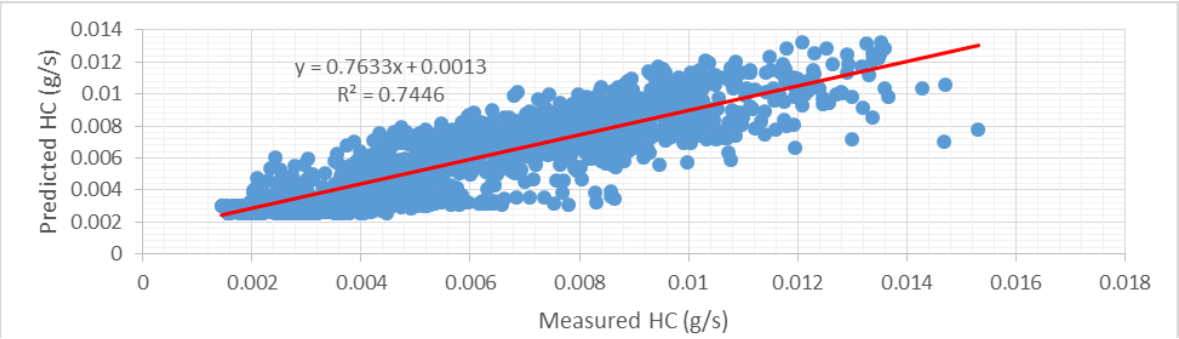

(b) VT-CPFM

Figure 18: Comparison between (a) CMEM and (b) VT-CPFM of HC estimates

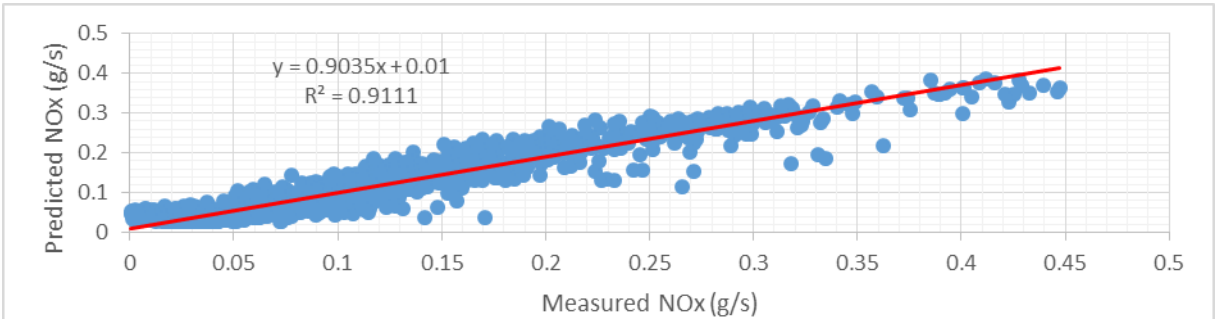

(a) CMEM

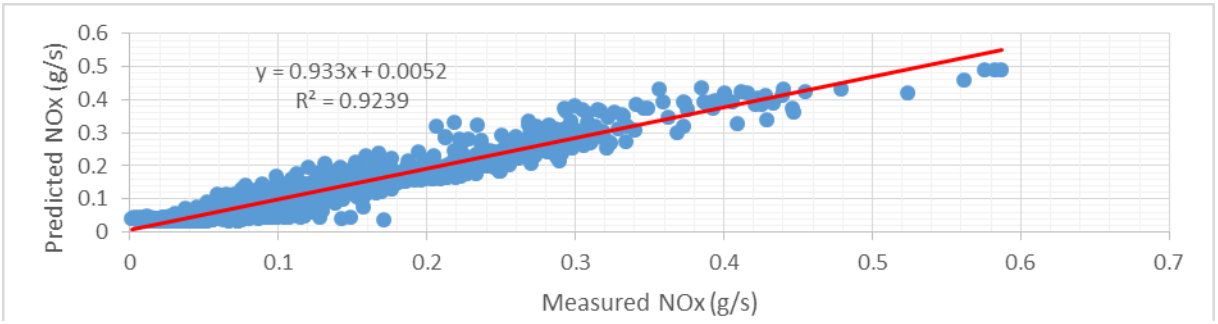

(b) VT-CPFM

Figure 19: Comparison between (a) CMEM and (b) VT-CPFM of NO_x estimates

Figure 17, Figure 18, Figure 19 illustrate the correlation of estimated emissions from CMEM and VT-CPFM with in-field measurements from HDDT 1. NO_x, the key target emission and the main concern in HDDT emissions, is highly correlated compared with CO and HC emissions. Moreover, VT-CPFM had better estimates for NO_x, CO, and HC compared to CMEM based on the R^2 values. The VT-CPFM estimated emissions are uniformly scattered and have better distribution around the regression line than CMEM. This is additional evidence that VT-CPFM provides better fuel estimates than CMEM.

Table 20: Average MAE and SMAPE for CMEM and VT-CPFM

Emissions	CMEM		VT-CPFM	
	MAE	SMAPE	MAE	SMAPE
CO	0.021786	0.54016	0.017014	0.455586
HC	0.000888	0.21699	0.000732	0.193229
NO_x	0.023443	0.24979	0.022614	0.246200

The performance of the model was further investigated and analyzed by estimating mean absolute error (MAE) and symmetric mean absolute percentage error (SMAPE) for CO, HC, and NO_x estimates (Table 20**Error! Reference source not found.**). MAE and SMAPE were calculated for vehicle trips estimated by the VT-CPFM and CMEM model structure to compute the difference in estimates against in-field measured data. SMAPE can be used as an alternative to mean absolute percentage error (MAPE) when there are zero or near-zero values in the data, which could result in infinitely high error rates that will increase the average error rate and will not represent the correct value. SMAPE was used as benchmark for the two models since some of the emissions values were near-zero. SMAPE yields higher error rates than usual due to the near-zero values but it limits the error to 200% as shown in Eq.

$$\boldsymbol{SMAPE} = \left| \frac{\boldsymbol{A_t - F_t}}{\frac{\boldsymbol{A_t + F_t}}{\boldsymbol{2}}} \right| \quad (16),$$

Where $\boldsymbol{A_t}$ is the actual value and $\boldsymbol{F_t}$ is the forecast value at time $\boldsymbol{t}$.

$$\boldsymbol{SMAPE} = \left| \frac{\boldsymbol{A_t - F_t}}{\frac{\boldsymbol{A_t + F_t}}{\boldsymbol{2}}} \right| \quad (\mathbf{16})$$

NO_x had an approximately similar SMAPE for both models, although SMAPE and MAE for CMEM were slightly higher than for VT-CPFM. The HC and CO error rates were higher for CMEM than for VT-CPFM, which corroborates the evident goodness of fit of VT-CPFM over CMEM.

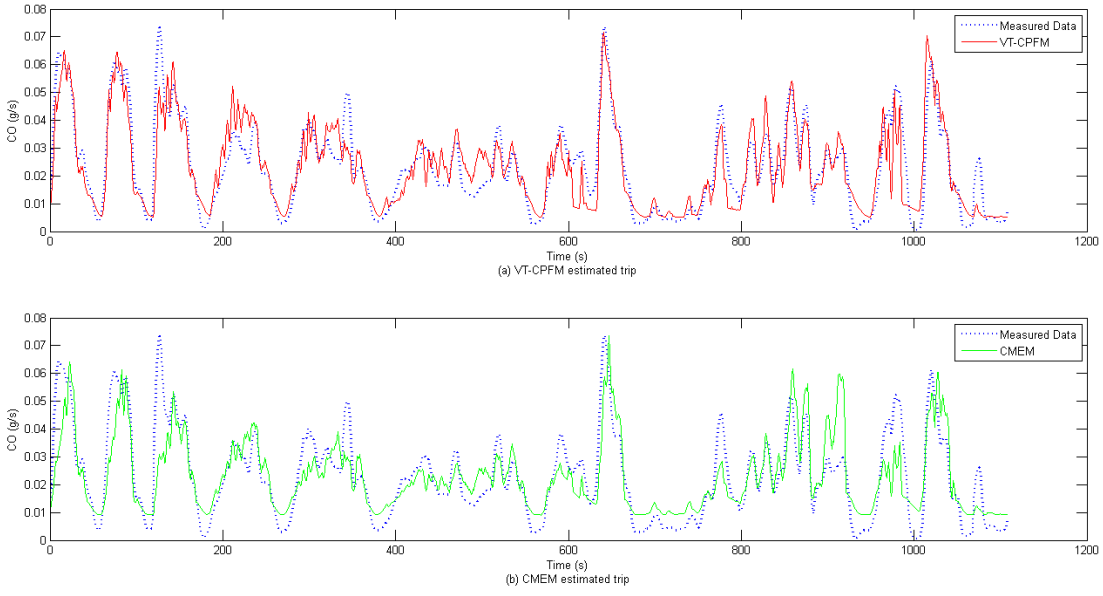

Figure 20: Model validation and comparison with CMEM for CO.

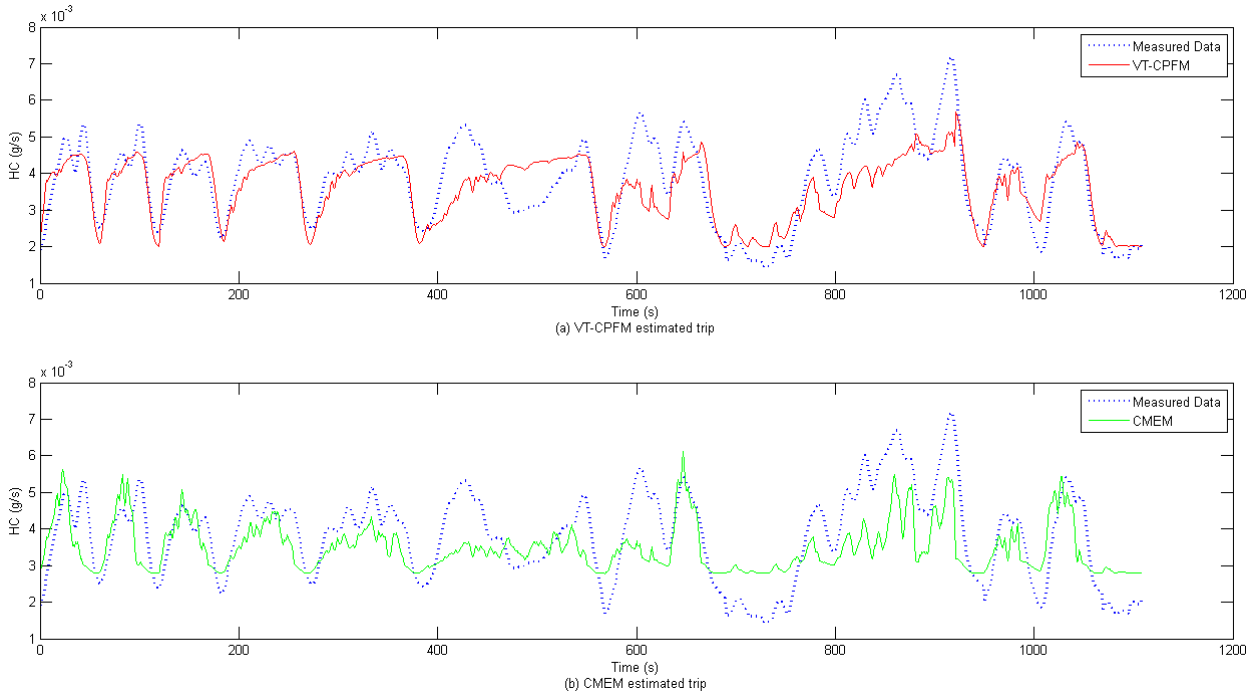

Figure 21: Model validation and comparison with CMEM for HC.

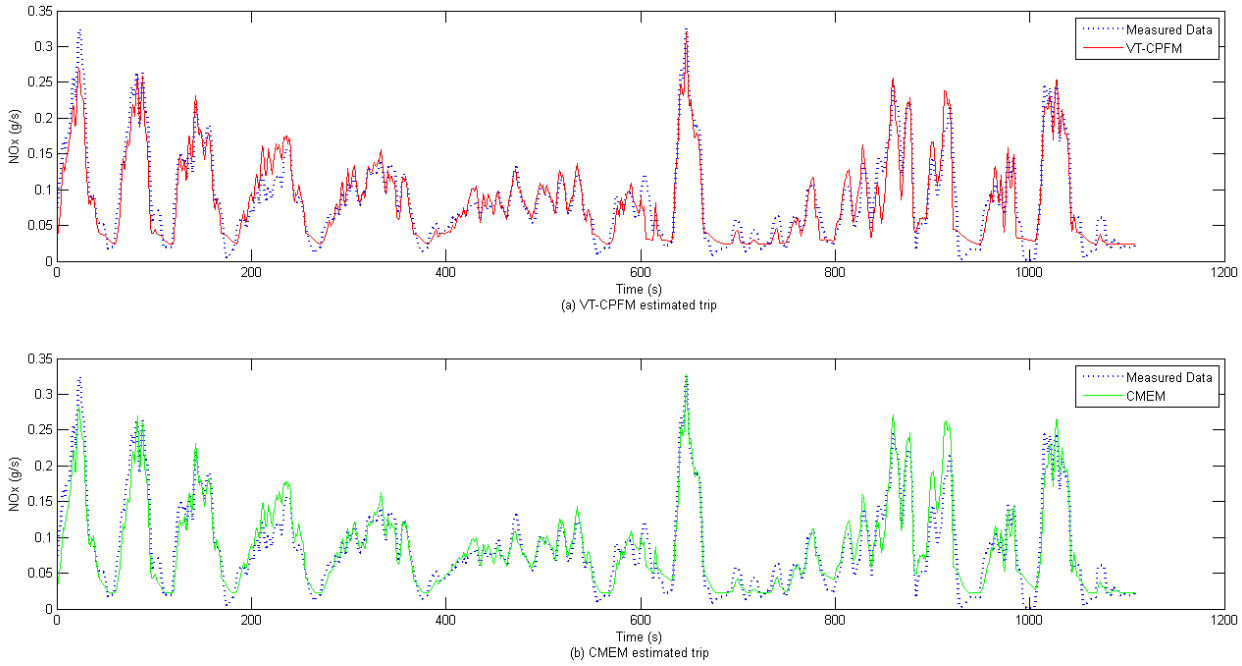

Figure 22: Model validation and comparison with CMEM for NOx.

Figure 20, Figure 21Figure 22 show sample estimated instantaneous emissions of the two models along with in-field measured data. The figures illustrate the ability of the models to capture the transient behavior of the three pollutants. The high error rates, which correspond to near-zero values are interpreted by the figures showing the large drops in empirical data. For NO_x, the two models were similar and fit the measured data well. The VT-CPFM model had better estimates for CO and HC, especially at lower values, where CMEM overestimates the emissions at these values. The VT-CPFM estimates were more consistent with in-field measured data for the three pollutants, specifically for HC and CO, which was expected from the demonstrated goodness of fit of the VT-CPFM model in previous tables and figures.

Light Duty vehicles (LDVs) Emission Modeling Results

Figure 23 illustrates the significant relationship between fuel consumption and emissions, showing that emissions follow the same behavior as fuel consumption. HC and CO emissions have a direct relationship with fuel consumption—as fuel consumption increases, emissions increase accordingly. This relationship is explained by the fact that HC and CO are the main components of gasoline, which consists of approximately 85% carbon and 15% hydrogen. The proposed model strongly fits the dataset for CO, HC and NO_x relatively. As expected, the highest levels of fuel consumption correspond to the highest levels of HC and CO emissions; this is a result of fuel enrichment at these high levels. Furthermore, NO_x emissions follow a general trend of increasing as they move towards a stoichiometric ratio where they reach a peak level then decrease afterwards during fuel enrichment. The aforementioned results make it evident that vehicle emissions directly relate to fuel consumption levels. Also notable is the significant relation of the fitted model to the emissions data. In addition, the model is consistent with CO, HC and NO_x since it maintains the same structure, using the same number of parameters and coefficients.

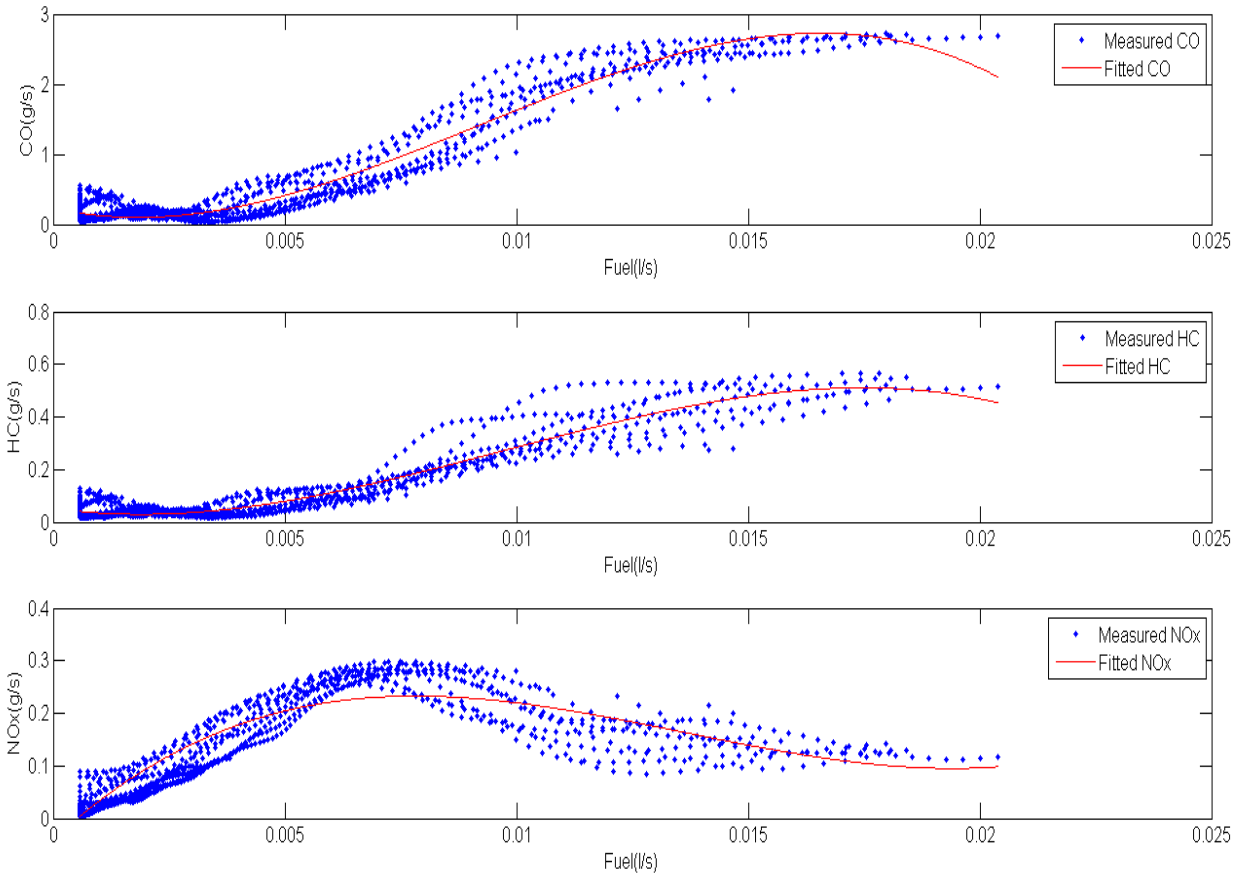

Figure 23: Fitting the Model to Oldsmobile Eighty Eight Emission Data

Regression analysis was implemented on the nine vehicles in the study to determine the model's accuracy in estimating emissions. Table 21 demonstrates the coefficient of determination (R^2) for each vehicle's emissions. The model showed a good fit for CO and HC, both when using the speed parameter and when excluding it. NO_x also had a relatively good fit for the model both with and without the speed parameters (R^2=0.802 and 0.828 respectively), as shown in Table 22. Table 22 also summarizes the average R^2 for CO and HC values, showing that including speed parameters (R^2 = 0.923 and 0.921 respectively) resulted in a slightly better fit than not using the speed parameters (R^2= 0.944 and 0.942 respectively). As these results show, there is only a slight increase in R^2 between the simpler model, which does not use the speed parameter, and the model that includes the speed parameter, indicating the negligible effect of speed on the model. Table 23 and Table 24 summarize sample model coefficients for estimating CO, HC and NO_x rates for the Oldsmobile Eighty-Eight.

Table 21: Coefficient of determination according to adding or excluding speed variable

Make/Model	Without Speed parameter			With Speed parameter		
	CO	HC	NO_x	CO	HC	NO_x
Toyota Celica	0.917	0.913	0.538	0.929	0.931	0.591
Geo Prizm	0.936	0.933	0.886	0.960	0.961	0.890
Subaru Legacy	0.939	0.939	0.837	0.957	0.960	0.841
Chevrolet Corsica	0.924	0.904	0.627	0.957	0.935	0.677
Oldsmobile Eighty Eight	0.950	0.922	0.895	0.958	0.936	0.902
Oldsmobile Cutlass Supreme	0.941	0.949	0.808	0.956	0.955	0.863
Mercury Villager Van	0.867	0.878	0.737	0.914	0.916	0.762
Jeep Grand Cherokee	0.942	0.956	0.930	0.952	0.963	0.951
Chevrolet Silverado	0.889	0.897	0.962	0.910	0.921	0.973

Table 22: Regression Model Comparison

Model	CO	HC	NO_x
With Speed	0.923	0.921	0.802
Without Speed	0.944	0.942	0.828

The accuracy of the model was further evaluated by comparing the instantaneous emission estimates to in-field measurements to examine their relationship and behavior. Figure 24 illustrates the fitted regression to the scattered data points used to estimate R^2. The predicted emission levels were highly correlated with the in-field measured data. Moreover, the R^2 values were approximately the same when the speed parameter was added and when only the fuel parameter was used. The two models follow similar trends for each emission, which implies that introducing the speed parameter into the model will produce approximately the same emission estimates based on fuel consumption.

Table 23: Sample Coefficients for Oldsmobile Eighty Eight Emissions (with speed parameters)

Old	Constant	v	F	v.F	F^2	v. F^2	F^3	v.F^3
CO	0.092	0.003	-70.712	-1.888	42790.00	141.752	-1.80E+06	-1727.70
HC	0.014	0.001	4.008	-0.549	3505.80	74.384	-1.55E+05	-2205.30
NO_x	-0.0505	2.20E-04	89.4688	-0.2207	-7661.00	21.5654	1.50E+05	-282.71

Table 24: Sample Coefficients for Oldsmobile Eighty Eight Emissions (without speed parameters)

Old	Constant	F	F^2	F^3
CO	0.234	-150.551	45499.00	-1.65E+06
HC	0.053	-25.599	7430.80	-2.56E+05
NO_x	-0.040	80.696	-7237.90	1.77E+05

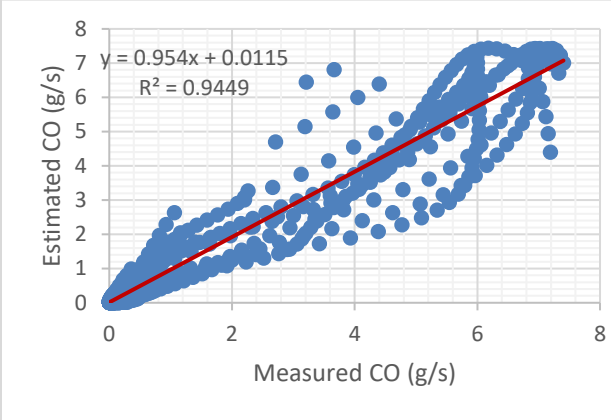

(a) Model without Speed variable.

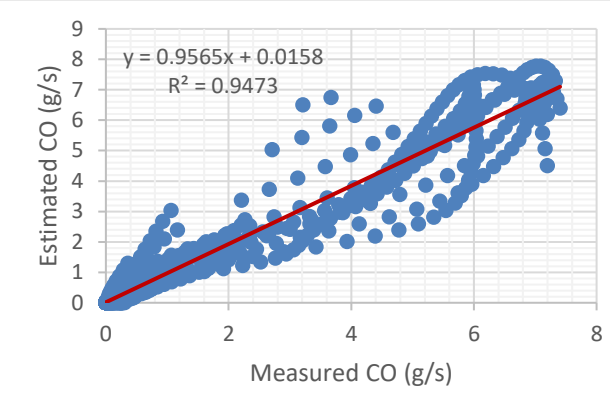

(b) Model with Speed variable.

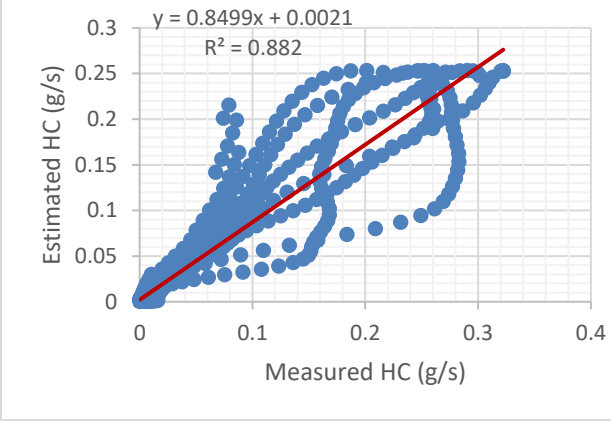

(c) Model without Speed variable.

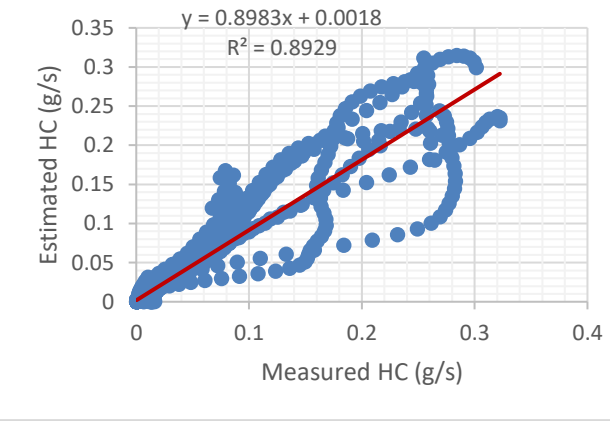

(d) Model with Speed variable.

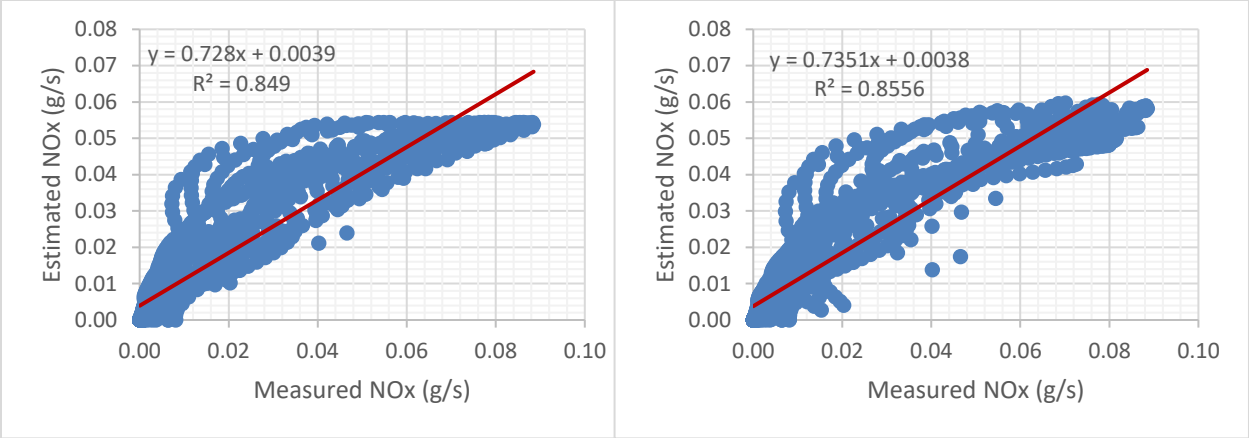

(e) Model without Speed variable. **(f) Model with Speed variable.**

Figure 24: Correlation between Measured estimated emission rates (Oldsmobile Eighty Eight)

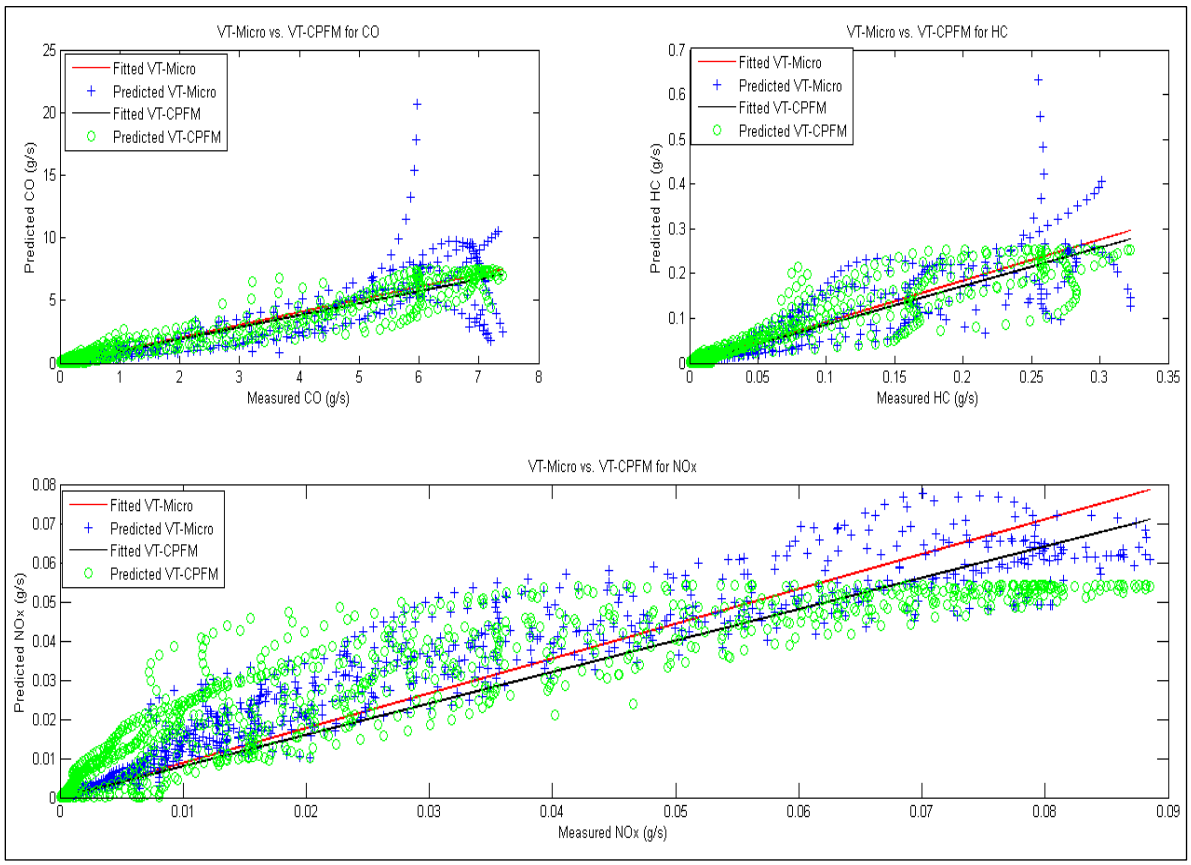

Figure 25: VT-Micro Vs. VT-CPFM

The model's performance was also evaluated by comparing its estimates to the VT-Micro model. Figure 25 demonstrates the correlation between a sample of the Oldsmobile Eighty-Eight's instantaneous in-field measurements and estimated emissions from VT-Micro and VT-CPFM models. As Figure 25 shows, the VT-CPFM emission model follows the same trend in predicting the emissions. The fitted regression lines for both models reveal the accuracy of the resulting estimates. VT-CPFM had a better fit for CO compared to VT-Micro for the Oldsmobile Eighty-Eight (R^2 = 0.945 and 0.82 respectively) as well as better estimates for HC (R^2 = 0.882 and 0.84 respectively). However, VT-Micro estimated NO_x with a higher R^2 of 0.922 compared to the VT-CPFM model's R^2 of 0.85. Note, though, that VT-Micro utilizes 32 coefficients incorporated within two boundary conditions to predict emission levels as compared to the VT-CPFM model, which uses only four calibrated coefficients at approximately the same level of accuracy. From these results, we can conclude that, overall, VT-CPFM returns good regression fit results for HC and CO over NO_x, which affirms the applicability of the VT-CPFM model to estimate emissions alongside fuel consumption.

The performance of the model was further investigated by calculating the mean absolute percentage error (MAPE) for the 9 vehicles for 16 driving cycles. Table 25 illustrates the error in trip emissions across 16 driving cycles for CO, HC and NO_x. Specifically, the error did not exceed 16.5% for the 16 driving cycles.

Table 25: Error in Trip Emissions

Driving Cycle	Error(%)		
	CO	HC	NOx
The City Test (LA04)	9.80%	10.35%	10.76%
Arterial LOS A (ARTA)	6.55%	8.90%	14.44%
Arterial LOS C (ARTC)	10.28%	10.33%	12.70%
Arterial LOS E (ARTE)	13.49%	11.35%	15.14%
Freeway High Speed (FWYSP)	8.57%	8.51%	20.23%
Freeway LOS A (FWYA)	9.15%	7.48%	16.50%
Freeway LOS D (FWYD)	7.04%	6.27%	16.46%
Freeway LOS E (FWYE)	5.17%	6.70%	11.20%
Freeway LOS F (FWYF)	5.25%	9.54%	9.00%
Freeway LOS G (FWYG)	13.73%	11.94%	10.26%
Local (LOCL)	12.26%	10.10%	11.19%
RAMP	5.17%	2.41%	8.68%
ST01	6.42%	8.50%	10.95%
AREA	7.54%	7.35%	11.49%
LA92	4.23%	4.06%	8.19%
New York Cycle (NYC)	5.55%	6.61%	15.65%
Average	8.14%	8.15%	12.68%

Electric Vehicles

After calibrating the model, the regenerative energy efficiency at any instant t ($\boldsymbol{\eta_{rb}(t)}$) is computed as a function of the instantaneous deceleration using Eq. (17); namely, the resulting model parameter $\boldsymbol{\alpha = 0.0411}$, as illustrated in Figure 26.

$$\eta_{rb}(t) = \begin{cases} \left[e^{\frac{0.0411}{|a(t)^-|}}\right]^{-1}, & \forall a(t) < 0 \\ 0, & \forall a(t) \geq 0 \end{cases} \quad (17)$$

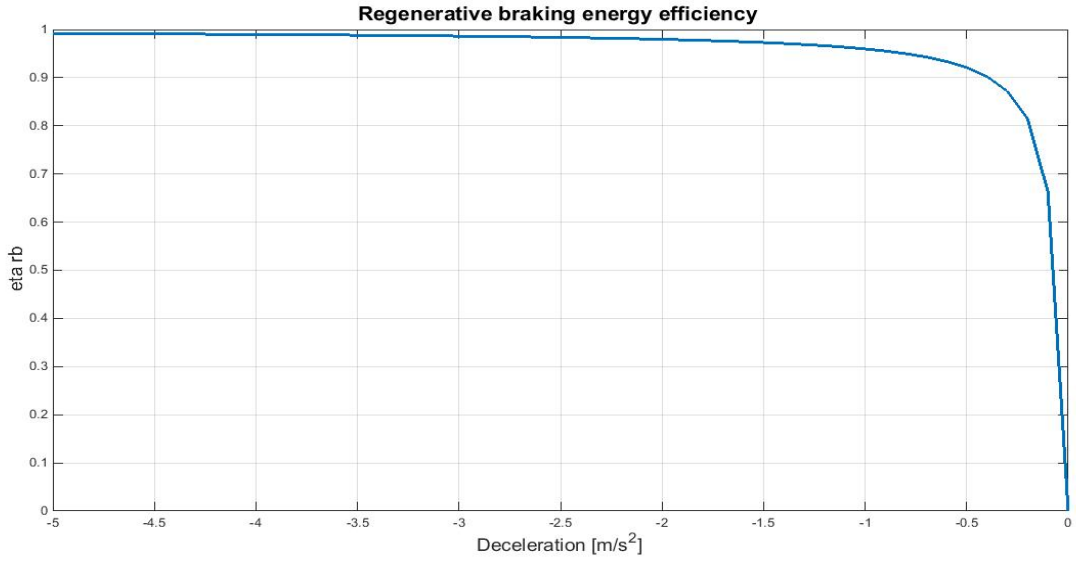

Figure 26: Electric LDV instantaneous regenerative efficiency vs. deceleration level

In Figure 27 the speed, power and SOC profiles for the WMTC driving cycle are shown. As illustrated in Figure 27a, when the vehicle decelerates, the electric power is negative. In this mode of operation, the energy flows from the wheels to the motor and charges the batteries, thus in these phases the SOC increases.

Moreover, in Figure 27a, the light blue area represents the energy consumed for the driving cycle. In particular, the portion of the area delimited by the blue line (positive quarter of the electric power graph) represents the case without energy regeneration during braking, while the red line (negative quarter of the electric power graph) shows the results considering the energy regeneration. As expected, the SOC increases while the vehicle is braking (red line) and produces a higher SOC compared to the no recovery case (blue line). The ability to recover energy during braking reduces the overall energy consumption, and thus the final SOC level is higher.

Figure 27 b shows the results of an example introduced to highlight the advantage of the energy recovery during braking events. A segment of 12 s of the WMTC cycle is analyzed for this purpose. The final SOC level without considering the regeneration is 94.91% while considering it is 94.84%. Consequently, when regeneration is considered, an increase of 0.07% in the final level of SOC is observed for these 12 s of the WTMC cycle. Moreover, if regeneration is not considered, net energy consumption is 39.4 [Wh] over 177.5

m, an energy efficiency of 222.1 [Wh/km]. When accounting for regenerative breaking, 17.5 [Wh] of energy is recaptured, resulting in a net energy consumption of 21.9 [Wh] and an energy efficiency of 123.3 [Wh/km]. The total energy consumption is computed by subtracting the energy recovered due to the use of regenerative braking from the energy used during traction, as a result the total energy consumed decreases.

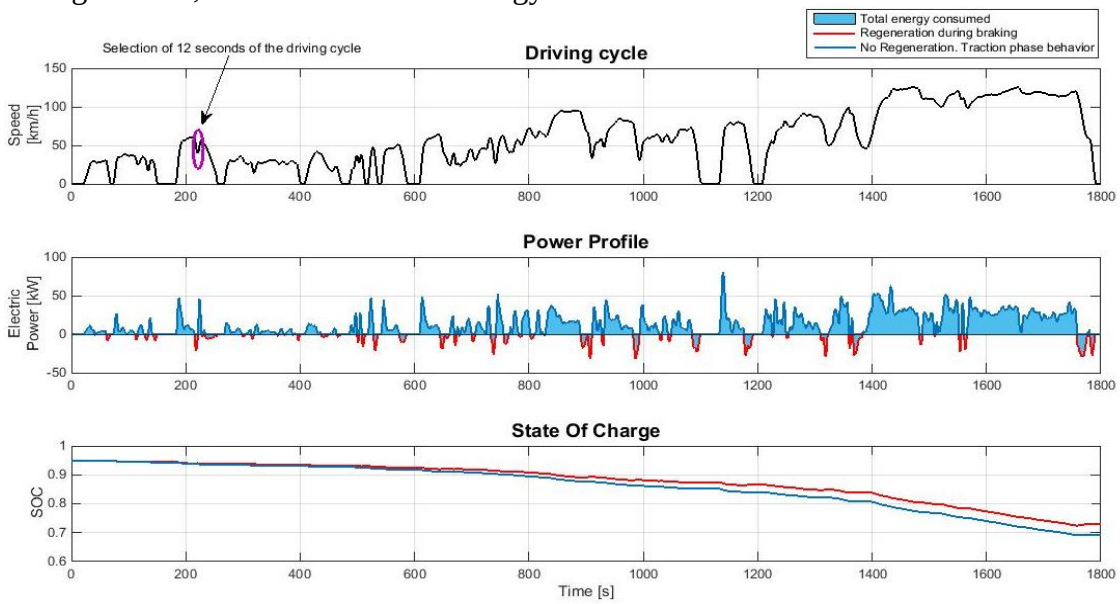

(a) WMTC driving cycle: speed, electric power and state of charge profiles on the entire cycle.

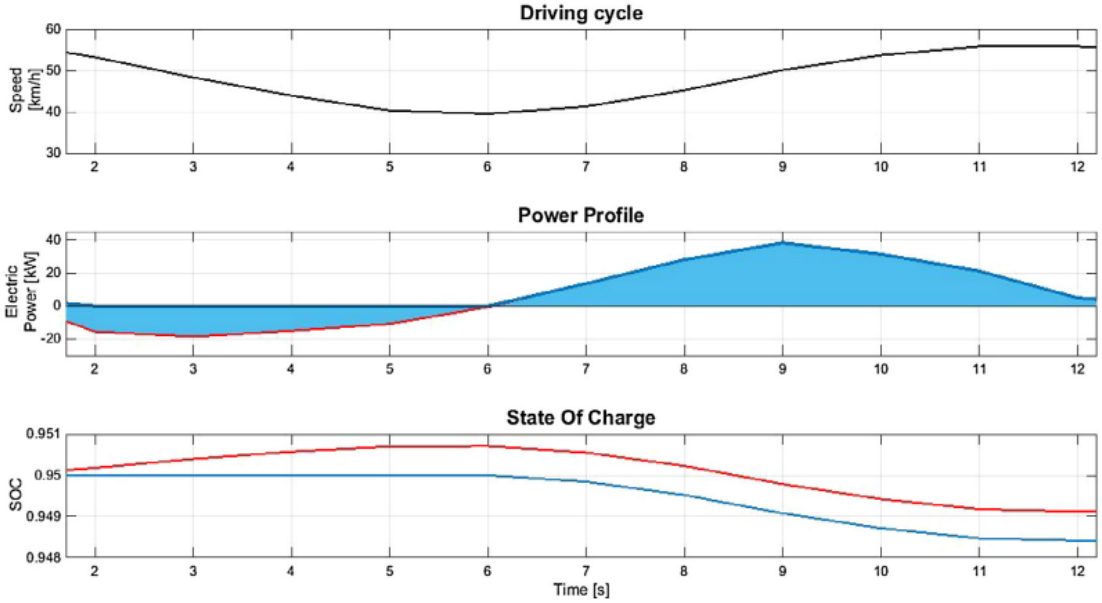

(b) WMTC driving cycle: speed, electric power and state of charge profiles on selected 12 seconds of the cycle.

Figure 27: WMTC driving cycle: speed, electric power and state of charge profiles

Table 26 reports the energy consumption in [Wh/km] and [Wh/mile] available by the JRC and by DOE's AVTA, and the energy consumption evaluated using the VT-CPEM model. In the last column of the table the error relative to the JRC and DOE's AVTA values is reported. The results indicate that the proposed model accurately estimates the energy consumption with an average error of 5.86% compared to the field data. Moreover, the consumption for the low speed range (speed $\leq$60 km/h) in the following driving cycles is analyzed: NEDC, WLTC and WMTC. Table 27 provides the characteristics and the consumptions in [Wh/km] for the low and high speed range cycles.

The average error, computed as the difference between the field data and the estimated consumption values, for the low speed range is 11.87%, while for the high speed range is 3.2%. The average error related to the low speed range results are higher than the error related to the high speed range. It is important to note, as shown in Table 27, that the traveled distance for the low speed range of every driving cycle analyzed are significantly lower when compared with the traveled distance for the high speed range. These distances are the "weights" in the evaluation of the error related to the average consumption on the entire driving cycle. For this reason the average error on the entire six driving cycles analyzed is 5.86%, thus lower than 11.87%.

Table 26: Electric LDV Model Validation Results

	AVTA/JRC data		VT-CPEM model		Error [%]
	[Wh/miles]	[Wh/km]	[Wh/miles]	[Wh/km]	
Nissan Leaf					
AVTA					
UDDS	201.4	125.1	233.8	145.3	16.11
HWFET	240.8	149.6	241.7	150.2	0.38
US06	321.6	199.8	347.9	216.2	8.19
JRC					
NEDC	252.7	156.9	239.0	148.5	-5.35
WLTC	287.3	178.4	273.3	169.8	-4.82
WMTC	294.5	182.9	293.4	182.3	-0.33

Table 27: Driving cycle characteristics and Nissan Leaf energy consumption levels

	Distance [km]	Duration [s]	Avg. speed [km/h]	Max speed [km/h]	AVTA/JRC [Wh/km]	VT-CPEM [Wh/km]	Error [%]
WLTC low speed	3.09	589	18.89	56.5	158	140.6	-11.01
WMTC low speed	4.06	600	24.4	60	169	142.4	-15.74
NEDC low speed	4.06	780	18.35	50	144.3	131.5	-8.87
WLTC high speed	20.17	1211	59.95	131.3	181.78	174.3	-4.11

WMTC high speed	24.84	1200	74.55	125.3	185.31	188.9	1.94
NEDC high speed	6.95	400	62.44	120	164.1	158.3	-3.53
WLTC	23.26	1800	46.5	131.3	178.4	169.8	-4.82
WMTC	28.9	1800	57.83	125.3	182.9	182.3	-0.33
NEDC	11.01	1180	33.21	120	156.9	148.5	-5.35

To evaluate the advantages of using electric vehicles with respect to conventional ones, a comparison on 16 driving cycles between the results of energy consumption obtained using the VT-CPEM and those using the VT-CPFM, on a similar gasoline vehicle, is reported. The results evaluated for the Nissan Versa in the VT-CPFM are used for comparison and shown in Figure 28. The results show that the on-board consumption of EVs are significantly lower than the consumption of similar conventional vehicles. This result is attributed to a number of factors including the higher energy efficiency through the use of on-board electric devices and the ability of electric vehicles to recover energy while braking. This analysis, known in the literature as tank-to-wheels (TTW) analysis, considers only energy use and emissions associated with vehicle operation activities, neglecting the energy use and emissions associated with fuel production. In the general framework the TTW is part of a more global and complex analysis named the well-to-wheels (WTW) analysis. In the WTW analysis the energy use and emissions associated with fuel production activities are evaluated using an analysis named well-to-tank (WTT), while the energy use and emissions associated with the vehicle operation activities are evaluated using the TTW analysis [38]. The WTT component of the WTW analysis is significantly higher for electricity than for gasoline. For this reason, the WTW analysis shows different results and a lower gap between the energy consumption of an electric and a conventional vehicle. Generally, the WTW analysis is influenced by many factors such as the efficiency of the energy production, transportation and distribution processes in the specific country and the specific energy carrier (e.g. electricity, gasoline, etc.) considered.

Figure 28 also shows that the EVs consume on average Electric vehicles, as with conventional ones, have a number of auxiliary systems. Some of them, such as the power steering and power brakes, have a minor impact on the vehicle energy consumption and range. However, the heating and air conditioning systems can have a dramatic impact on the energy consumption and range of electric vehicles. The impact of auxiliary systems on the energy consumption of a vehicle is a topic that is of significant interest in recent years. Moreover, the evaluation of this impact is very important in computing the EV range. Specifically, the higher the impact of the auxiliary system load has, the higher is the energy consumption [Wh/km] and the lower is the available distance that can be driven using the electric vehicle [39]. A study by the National Renewable Energy Laboratory (NREL) concluded that a reduction on the EV range of up to 38% was possible [40]. The study investigated the impact of the auxiliary systems on the Nissan Leaf using data collected from a previous study. Specifically, the data were collected on 7375 trips using Nissan Leaf vehicles with outside temperatures recorded. The total auxiliary system load considered includes: cabin heater and fan, component heaters (ie. battery heater), headlights, power steering, radio etc. A comfort temperature range between 15℃ and 24 ℃ in the cabin was set.

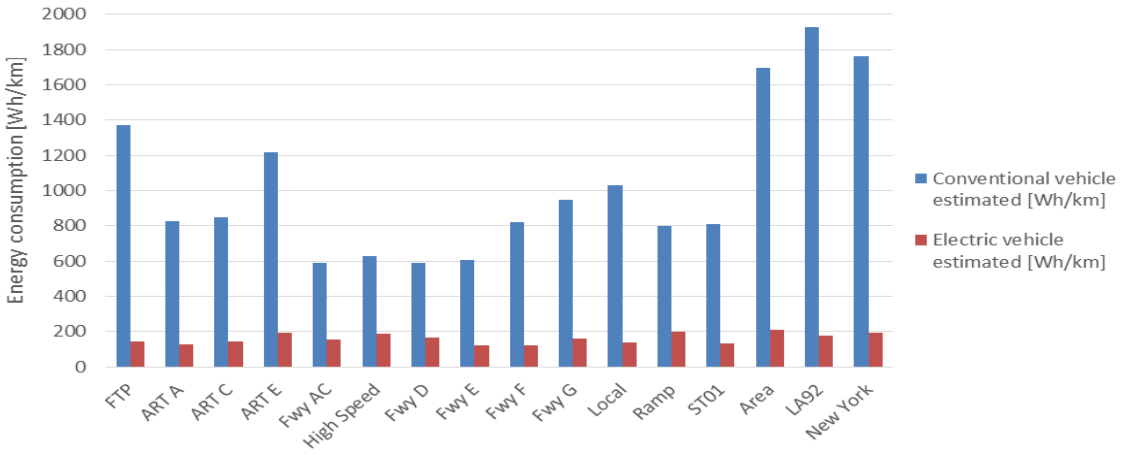

Figure 28: Comparison between the energy consumption estimated values of Nissan Leaf and Nissan Versa.

In the VT-CPEM model, a base auxiliary system load of 700 [W] is considered. In this section, three different scenarios are analyzed and compared with the case of a base auxiliary load of 700 [W]. In particular, the outside temperatures of: 25 ℃, 35 ℃ and -5 ℃ are considered. On the basis of the data reported by [39], the total auxiliary system loads are 850 [W], 1200 [W] and 2200 [W], respectively. Table 28 demonstrates the results of the impact of the auxiliary load on the energy consumption for 25 ℃, 35 ℃ and -5 ℃ ambient temperatures.

The simulation results indicate that the UDDS is the most affected drive cycle by the auxiliary load on the energy consumption, with an energy consumption increase of 32% when the outside temperature is -5 ℃. On the contrary, the US06 cycle is the least affected driving cycle by the heating system usage with a 10% increase in the energy consumption. These two cycles are also those with the highest and the lowest energy consumption levels, respectively. This result demonstrates that generally the higher the energy consumption [Wh/km], the lower is the impact of the auxiliary systems. These systems, in fact, represent a constant additional load for the vehicle. Also the study demonstrated that the absolute temperature differences from the base condition, between 15℃ and 24 ℃, might correlate to the higher energy consumption of 35 ℃ and -5 ℃ ambient temperatures. The table demonstrates that a 20 ℃ difference (-5 ℃) consumes 20.3% more energy and a 10 ℃ difference utilizes 6.7% more energy.

Table 28: Impact of auxiliary systems load on the consumption at: 25 ℃, 35 ℃ and 5 ℃.

Consumption	700 W	850 W [25 ºC]		1200 W [35 ºC]		2200 W [-5 ºC]	
	[Wh/km]	[Wh/km]	Increase from 700 W [%]	[Wh/km]	Increase from 700 W [%]	[Wh/km]	Increase from 700 W [%]
UDDS	145	150	3	161	11	192	32
HWFET	150	153	2	158	5	175	16
US06	216	218	1	223	3	238	10
NEDC	149	153	3	163	9	190	28
WLTC	170	173	2	181	7	204	20
WMTC	182	185	2	192	5	211	16

Electric Trains

The resulting model generates the regenerative efficiency model parameter of 0.65 ($\alpha = 0.65$), as demonstrated by Figure 29 to present a decay with the decrease of deceleration level. In particular, the decay becomes dramatic when the deceleration is less than 2 m/s^2.

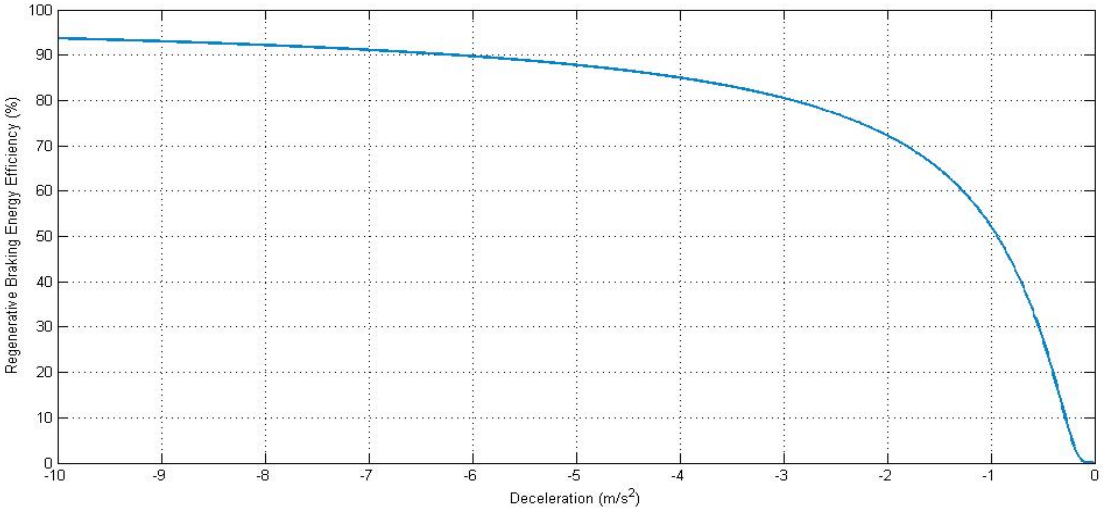

Figure 29: Electric train instantaneous regenerative efficiency vs. deceleration level

The model was validated at an aggregated level by comparing trip-based model estimates against the NTD system averages. Table 29 presents the model validation results. Basically, the model can generate consistent results by incorporating the instantaneous regenerative efficiency, resulting in an estimate of 37.12 *kWh/VM* and 0.127 *kWh/SM* which produces a prediction error of only 1.87% and -2.31% respectively. Failing to capture energy recovery, as shown in the table (no regeneration) results in a significantly high bias of model estimates. Noteworthy here is that the presumption of the constant regenerative efficiency results in larger deviation of estimation than the proposed model, although it outperforms the "no regeneration" case.

Table 29: Electric Train Model Validation

	Empirical energy	Instantaneous regeneration		Constant regeneration		No regeneration	
		Energy estimates	Error (%)	Energy estimates	Error (%)	Energy estimates	Error (%)
kWh/VM	36.44	37.12	1.87	42.31	16.11	46.42	27.39
kWh/SM	0.13	0.127	-2.31	0.144	10.77	0.158	21.54

Figure 30 illustrates the speed, instantaneous and cumulative energy consumption for the driving cycle. The light blue area represents the energy consumed for the entire cycle. The area delimited by the blue edge line refers to the energy consumed during acceleration which cannot be regenerated, and the red edge line represents the energy consumption resulted from braking. As expected, energy is recovered during braking, resulting in lower

energy consumption levels compared to "no regeneration" case. The cumulative energy consumption demonstrates that the ability to recover braking energy significantly reduces the overall energy consumption for the entire trip.

To quantify the energy saving, the trip-based model estimates were compared between the proposed model and the "no regeneration" case, resulting in Table 30. Basically, the proposed model produces the trip-based energy consumption significantly lower than that of "no regeneration" case, resulting in an average energy saving of 20.03%.

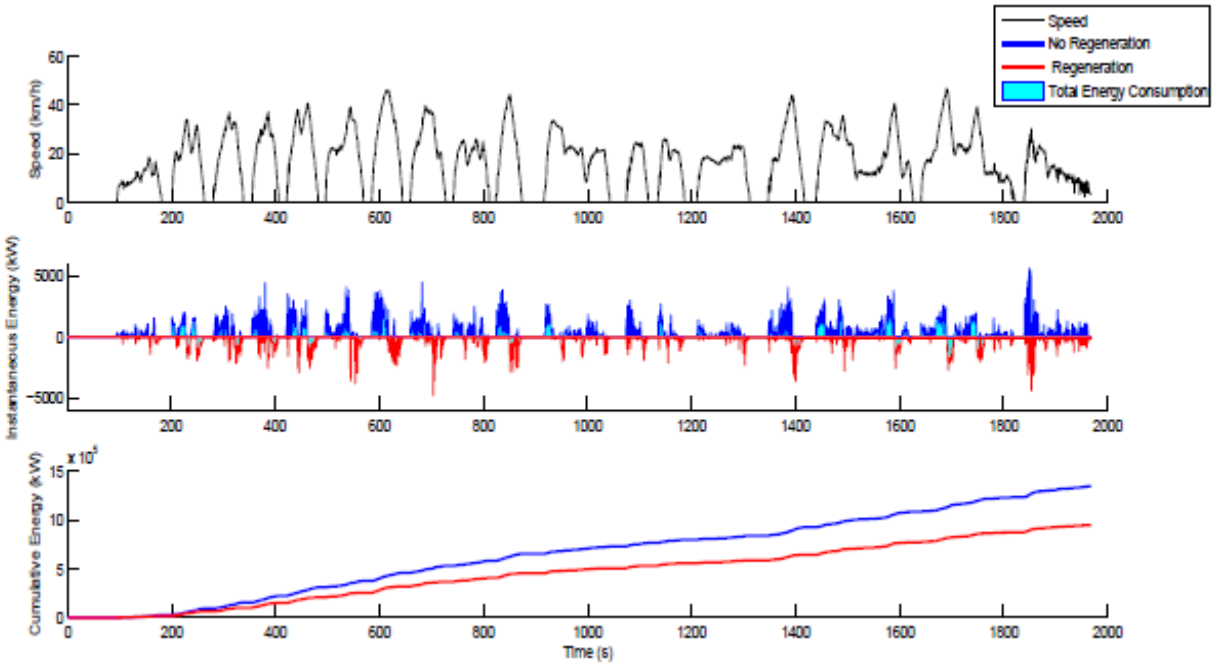

Figure 30: Speed and electric power on the entire cycle

Table 30: Energy Savings Resulted from Energy Regeneration

Energy Consumption (instantaneous regeneration, kWh/VM)	37.12
Energy Consumption (no regeneration, kWh/VM)	46.42
Energy saving (%)	20.03

CONCLUSIONS AND RECOMMENDATIONS

The study develops energy/fuel consumption and emission models for multiple vehicle modes and rail trains in support of environmentally sustainable transportation systems, such as eco-routing, eco-driving, eco-transit, and eco-freight programs. Given that conventional gasoline-powered LDVs have been modeled by previous studies, the proposed study mainly focuses on Heavy Duty Vehicles (HDVs) and new energy vehicles. Specifically, electric LDVs and trains, conventional diesel, hybrid-electric and compressed natural gas (CNG) buses as well as heavy duty diesel trucks are thoroughly investigated.

The models are developed based on VT-CPFM for the fuel-powered vehicles and on VT-CPEM for the electric energy vehicles and trains. The VT-CPFM modeling framework characterizes fuel consumption as a second-order polynomial function of vehicle power so that circumvent the bang-bang control in the modeling practice. The VT-CPFM fuel consumption model has also been extended to predict pollutant emissions (HC, CO, NO_x) for HDDTs and LDVs. The emission models are characterized as a polynomial function of fuel consumption and vehicle speed. The VT-CPEM modeling framework models the electric energy consumption as a polynomial function of vehicle speed and acceleration, and also instantaneously captures the energy regeneration resulting from braking by characterizing the recovered energy as a function of deceleration level. The models are validated by comparing estimated fuel/energy consumption and emissions against field observations and/or the estimates of other state-of-the-art models.

The results demonstrate that the proposed models can accurately predict energy/fuel consumption and emissions consistent with field measurements, and outperform other state-of-the-practice models in terms of circumventing bang-bang control and being calibrated using publicly available data. The resulting models will be used to develop eco-friendly strategies for multimodal transportation systems.

It is recommended that EPA requires heavy duty vehicles to report their fuel economy in the future so that the model can be calibrated using publicly available data without mass in-field data collection, which can maximize the cost-effectiveness of model development.

REFERENCES

1. Park, S., et al., *Virginia Tech Comprehensive Power-based Fuel Consumption Model (VT-CPFM): Model Validation and Calibration Considerations.* International Journal of Transportation Science and Technology, 2013. 2(4): p. 317-336.
2. Rakha, H.A., et al., *Virginia tech comprehensive power-based fuel consumption model: model development and testing.* Transportation Research Part D: Transport and Environment, 2011. 16(7): p. 492-503.
3. Davis, S.C., S.W. Diegel, and R.G. Boundy, *Transportation energy data book.* 2008.
4. EPA, A., *Inventory of US greenhouse gas emissions and sinks: 1990-2009*. 2011, EPA 430-R-11-005.
5. EPA, U., *User's Guide to MOBILE6. 1 and MOBILE6. 2.* Environmental Protection Agency, 2003.
6. Ahn, K. and H. Rakha, *The effects of route choice decisions on vehicle energy consumption and emissions.* Transportation Research Part D: Transport and Environment, 2008. 13(3): p. 151-167.
7. Rakha, H., K. Ahn, and A. Trani, *Development of VT-Micro model for estimating hot stabilized light duty vehicle and truck emissions.* Transportation Research Part D: Transport and Environment, 2004. 9(1): p. 49-74.
8. Hausberger, S., et al., *PHEM User guide for version 10.* TUG/FVT Report, 2010: p. 1-57.
9. Smit, R., R. Smokers, and E. Rabé, *A new modelling approach for road traffic emissions: VERSIT+*. Transportation Research Part D: Transport and Environment, 2007. 12(6): p. 414-422.
10. Barth, M., et al., *Development of a comprehensive modal emissions model*. 2000: National Cooperative Highway Research Program, Transportation Research Board of the National Academies.
11. Barth, M., G. Scora, and T. Younglove, *Modal emissions model for heavy-duty diesel vehicles.* Transportation Research Record: Journal of the Transportation Research Board, 2004(1880): p. 10-20.
12. Becker, T.A., I. Sidhu, and B. Tenderich, *Electric vehicles in the United States: a new model with forecasts to 2030.* Center for Entrepreneurship and Technology, University of California, Berkeley, 2009. 24.
13. Muratori, M., et al., *Highly-resolved modeling of personal transportation energy consumption in the United States.* Energy, 2013. 58: p. 168-177.
14. Wu, X., et al., *Electric vehicles' energy consumption measurement and estimation.* Transportation Research Part D: Transport and Environment, 2015. 34: p. 52-67.
15. Hayes, J.G., et al. *Simplified electric vehicle power train models and range estimation*. in *2011 IEEE Vehicle Power and Propulsion Conference*. 2011. IEEE.
16. Shibata, S. and T. Nakagawa, *Mathematical Model of Electric Vehicle Power Consumption for Traveling and Air-Conditioning.*
17. Abousleiman, R. and O. Rawashdeh. *Energy consumption model of an electric vehicle*. in *Transportation Electrification Conference and Expo (ITEC), 2015 IEEE*. 2015. IEEE.

18. Halmeaho, T., et al. *Electric City Bus Energy Flow Model and Its Validation by Dynamometer Test*. in *Vehicle Power and Propulsion Conference (VPPC), 2015 IEEE*. 2015. IEEE.
19. Messa, C., *Comparison of emissions from light rail transit, electric commuter rail, and diesel multiple units.* Transportation Research Record: Journal of the Transportation Research Board, 2006(1955): p. 26-33.
20. Puchalsky, C., *Comparison of emissions from light rail transit and bus rapid transit.* Transportation Research Record: Journal of the Transportation Research Board, 2005(1927): p. 31-37.
21. Barrero, R., X. Tackoen, and J. Van Mierlo. *Quasi-static simulation method for evaluation of energy consumption in hybrid light rail vehicles*. in *2008 IEEE Vehicle Power and Propulsion Conference*. 2008. IEEE.
22. Gbologah, F., et al., *Demonstrating a bottom-up framework for evaluating energy and emissions performance of electric rail transit options.* Transportation Research Record: Journal of the Transportation Research Board, 2014(2428): p. 10-17.
23. Jong, J.-C. and E.-F. Chang, *Models for estimating energy consumption of electric trains.* Journal of the Eastern Asia Society for Transportation Studies, 2005. 6: p. 278-291.
24. Liu, R.R. and I.M. Golovitcher, *Energy-efficient operation of rail vehicles.* Transportation Research Part A: Policy and Practice, 2003. 37(10): p. 917-932.
25. Mittal, R.K., *Energy Intensity of Intercity Passenger Rail*. 1977.
26. Fiori, C., K. Ahn, and H.A. Rakha, *Power-based electric vehicle energy consumption model: Model development and validation.* Applied Energy, 2016. 168: p. 257-268.
27. Rakha, H., et al., *Vehicle dynamics model for predicting maximum truck acceleration levels.* Journal of transportation engineering, 2001. 127(5): p. 418-425.
28. Fitch, J.W., *Motor truck engineering handbook.* Technology, 1994. 2004: p. 03-08.
29. Wong, J.Y., *Theory of ground vehicles*. 2001: John Wiley & Sons.
30. Edwardes, W. and H. Rakha, *Virginia Tech Comprehensive Power-Based Fuel Consumption Model: Modeling Diesel and Hybrid Buses.* Transportation Research Record: Journal of the Transportation Research Board, 2014(2428): p. 1-9.
31. Feng, C., *Transit bus load-based modal emission rate model development.* 2007.
32. Hay, W.W., *Railroad engineering*. Vol. 1. 1982: John Wiley & Sons.
33. Procedure, S., *J2188, Commercial truck and bus SAE recommended procedure for vehicle performance prediction and charting.* Society of Automotive Engineers, Warrendale, PA, 1996.
34. Cocker, D.R., et al., *Development and application of a mobile laboratory for measuring emissions from diesel engines. 1. Regulated gaseous emissions.* Environmental science & technology, 2004. 38(7): p. 2182-2189.
35. Gao, Y., L. Chu, and M. Ehsani. *Design and control principles of hybrid braking system for EV, HEV and FCV*. in *2007 IEEE Vehicle Power and Propulsion Conference*. 2007. IEEE.
36. De Gennaro, M., et al., *Experimental test campaign on a battery electric vehicle: laboratory test results (Part 1).* SAE International Journal of Alternative Powertrains, 2015. 4(2015-01-1167): p. 100-114.

37. Reşitoğlu, İ.A., K. Altinişik, and A. Keskin, *The pollutant emissions from diesel-engine vehicles and exhaust aftertreatment systems.* Clean Technologies and Environmental Policy, 2015. 17(1): p. 15-27.
38. Wang, M., T. Weber, and T. Darlington, *Well-to-wheels analysis of advanced fuel/vehicle systems—a North American study of energy use, greenhouse gas emissions, and criteria pollutant emissions.* Well-to-Wheels Analysis of Advanced Fuel/Vehicle Systems: A North American Study of Energy Use, Greenhouse Gas Emissions, and Criteria Pollutant Emissions, 2005.
39. Mebarki, B., et al., *Impact of the air-conditioning system on the power consumption of an electric vehicle powered by lithium-ion battery.* Modelling and Simulation in Engineering, 2013. 2013: p. 26.
40. Farrington, R. and J. Rugh. *Impact of vehicle air-conditioning on fuel economy, tailpipe emissions, and electric vehicle range*. in *Earth technologies forum*. 2000.